DROPLET-BASED MICROFLUIDIC SYSTEMS FOR SILICA COATING AND SYNTHESIS OF CONJUGATED POLYMER NANOPARTICLES

A THESIS SUBMITTED TO

THE GRADUATE SCHOOL OF ENGINEERING AND SCIENCE

OF BILKENT UNIVERSITY

IN PARTIAL FULFILLMENT OF THE REQUIREMENTS FOR

THE DEGREE OF

MASTER OF SCIENCE

IN

MECHANICAL ENGINEERING

By

Alican Özkan

July, 2015

Droplet-Based Microfluidic Systems for Silica Coating and Synthesis of Conjugated Polymer Nanoparticles
By Alican Özkan
July, 2015

We certify that we have read this thesis and that in our opinion it is fully adequate, in scope and in quality, as a thesis for the degree of Master of Science.

Asst. Prof. Dr. Emine Yegân Erdem(Advisor)

Asst. Prof. Dr. Barbaros Çetin

Prof. Dr. Zafer Dursunkaya

Approved for the Graduate School of Engineering and Science:

Prof. Dr. Levent Onural
Director of the Graduate School

ABSTRACT

DROPLET-BASED MICROFLUIDIC SYSTEMS FOR SILICA COATING AND SYNTHESIS OF CONJUGATED POLYMER NANOPARTICLES

Alican Özkan
M.S. in Mechanical Engineering
Advisor: Asst. Prof. Dr. Emine Yegân Erdem
July, 2015

Nanoparticles have unique electronic, optic and magnetic properties due to their large area to volume ratio. In order for them to preserve their properties for longer times, some of them need to be coated with a protective layer such as silica (silicon dioxide) layer. This coating has to be made uniformly to obtain monodisperse size distributions, which is essential to obtain uniform properties for all nanoparticles. Obtaining monodisperse size distribution relies on the control over reaction conditions such as residence time, concentration and temperature. This thesis presents a microfluidic reactor that can achieve strict control over reaction conditions by utilizing a meandering geometry of microchannels and droplet-based flow. Meandering channels reduce the time needed for mixing due to the reduced diffusion lengths; whereas droplet-based flow provides uniform residence time inside the reactor due to the circulating flow profile of droplets as opposed to parabolic flow profile in straight channels. Before fabricating the device, the mixing performance of droplets at different channel cross-sections and meandering geometries were simulated by using Comsol Multiphysics®. As a result, it is concluded that the channel cross-section and meandering dimensions should be as small as possible for faster mixing. Based on these simulation results, the microfluidic device was designed and later fabricated in polydimethyl siloxane (PDMS) by using the soft lithography technique. This system was used to understand the effect of solvent concentrations and residence time on silica formation in order to be able to control the coating thickness compared to batch-wise methods. Initially silica nanoparticle formation inside droplets were tested; and 102 nm ± 4 nm diameter of silica nanoparticles were obtained; which is a significant improvement compared to the bath-wise synthesis methods. Additionally, experimental studies on the synthesis of green Conjugated Polymer Nanoparticles (CPN) was also conducted. By using three different methods, bulk

solution, continuous flow and droplet-based flow, nanoparticles were synthesized. From the results, it was acquired that droplet-based flow provided higher quality of nanoparticles in terms of nanoparticle size, uniformity and monodispersity.

Keywords: Microfluidics, Droplet-Based Microfluidics, Microreactors, Silica Coating, Quantum Dots, Silica Nanoparticles, Conjugated Polymer Nanoparticle Synthesis, Particle Motion in Fluid Medium, Level Set Method.

ÖZET

NANOPARÇACIKLARIN DAMLACIK TABANLI MİKROREAKTÖR KULLANİLARAK SİLİSYUM DİOKSİT İLE KAPLANMASI VE KONJUGE POLİMER PARÇACIK SENTEZI

Alican Özkan
Makine Mühendisliği, Yüksek Lisans
Tez Danışmanı: Asst. Prof. Dr. Emine Yegân Erdem
Temmuz, 2015

Nanoparçacıklar, büyük yüzey alanı-hacim oranına sahip olduklarından özgün elektronik, optik ve manyetik özelliklere sahiptirler. Bu özelliklerin daha uzun süre boyunca korunması için silisyum dioksit (SiO_2) gibi koruyucu bir katmanla kaplanması gerekir. Bir örnek özelliklerde nanoparçacıklar elde etmek için nanoparçacıkların eş dağılımlı olması gerekir. Eş boyutlarda nanoparçacıkların sentezlenmesi, reaksiyon süresi, konsantrasyon ve sentez sırasındaki sıcaklık gibi reaksiyon koşullarına bağıdır. Bu tezde kıvrımlı mikrokanallardan oluşan ve damla bazlı akış sağlayabilen özellikleriyle belirtilen reaksiyon koşullarını sağlayabilen bir mikroreaktor sunulmuştur. Kıvrımlı kanallar karışma için gereken süreyi duşürme ve düzgün dağılma uzunluğu sağlayabilen; bununla birlikle düz akıştaki parabolik akış profilinin aksine damla bazlı akışın akış profili düzgün sirkülasyon süresi sağlar. Aletin üretiminden önce Comsol Multiphysics® kullanılarak karışma performansı farklı kesit alanı ve kıvrım geometrilerinde test edilmiştir. Sonuç olarak hızlı karışma için kıvrımlı kanallar olabildiğince küçük olması yargısına varılmıştır. Simülasyon sonuçlarına göre mikroreaktor tasarımı tamamlanmış ve soft lithografi tekniği kullanılarak kanallar PDMS'ten üretilmiştir. Bu sistem, solvent konsantrasyonu ve sirkülasyon süresinin etkisini anlamak ve kaplama kalınlığını kesikli duzeneklere göre kontrolunun ne denli iyi olduğunu anlamak için öncelikle silisyum formasyonunu test etmiştir. Öncelikli olarak damlaların içinde silisyum oluşumu test edilmiş ve 102 nm $\pm$ 4 nm boyutlarında nanoparçacıklar elde edilmiştir. Sentez süresini baz alarak kesikli düzeneklere göre önemli gelişimler olduğu görülmüştür. Buna ek

olarak benzer bir mikroreaktörde Konjuge Polimer Nanoparçacık (KPN) sentezi yapılmıştır. Konjuge Polimer Nanoparçacık sentezi üç farklı yöntem kullanırak sentezlenmiştir. Bunlar kesikli düzenek, düz akış ve damla bazlı akış yöntemleridir. Deney sonuçlarına göre damla bazlı akış yönteminin düz akış ve kesikli düzenek yöntemlerine göre parçacık boyutu, tekbiçimlilik ve tek dağılımlılık açısından daha başarılı olduğu gözlemlenmiştir.

Anahtar sözcükler: Mikroakışkanlar, Damla Bazlı Mikroakış, Mikroreaktörler, Silisyum Dioksit Kaplama, Silisyum Dioksit Nanoparçacık Sentezi, Nicem Noktaları, Level Set Metodu, Akış İçerisinde Parçacık Hareketi, Konjuge Polimer Nanoparçacık Sentezi.

Acknowledgement

First, I would like to thank my advisor Prof. Yegân Erdem. I am very pleased and satisfied from her support and contribution during this period of time. I am also thankful to her patience for reviewing my articles, including this thesis, and financial support for the needs in the manner of research and the conferences. It was a great opportunity to work together with her. Additionally, I would like express my sincere appreciations to Prof. Barbaros Çetin; who introduced me to this valuable topic, microfluidics six years ago, for his motivation and support throughout this period of time. I am also thankful to Prof. İlker Temizer for his support and patience during the Ph.D. application period. I am also grateful to Prof. Zafer Dursunkaya for his patience during thesis jury times.

Technical staff and students of National Nanotechnology Research Center (UNAM) has a great role for helping me to finish this work. Especially, Mehmet Yılmaz, Merve Marçalı, Yusuf Keleştemur, Hamidou Keita and Samad Nadimi had a great contribution by sparing their time during fabrication and analyzing results. Additionaly, I am grateful to Tayfun Akın from METU MEMS. and our collaborators Prof. Hilmi Volkan Demir and Prof. Dönuş Tuncel.

I would like to acknowledge to my valuable friends from Bilkent University Underwater Society (Bilsat), especially Merve Büyükbaş, Nilgün Dönmez, Volkan Kahrıman, Elif Dayı, Berk Abacı and Ayşegül Çanga morally supported me in Bilkent University. I would also like to thank to my precious friends Berkan Pakkanlılar and Mertcan Tarhan from METU–NCC and Serhat Kerimoğlu, Buğra Türeyen and Gökberk Kabacaoğlu from Bilkent University, Department of Mechanical Engineering for their mental support both for my research and my hard times in the loss of my beloved friend Merve Büyükbaş.

Last but not the least, I would like to acknowledge with my gratitude and love to my family Savaş Özkan, Fehime Özkan and Ömer Ege Özkan for supporting me and sharing my stress in every moment of my life. Without their encouragement, patience and valuable support, I would not be able to reach up to this point.

Dedicated to my family; Savaş, Fehime, Ömer Ege
and
my beloved friend; Merve Büyükbaş
may rest in peace.

Contents

List of Figures

List of Tables

Nomenclature

$d_{effective}$	Effective droplet diameter
F_{drag}	Drag force on spherical particle
F_{st}	Surface tension force
h	Length of the droplet
u	Flow velocity
u_{rel}	Relative velocity of particle
t	Time
$t_{corr.}$	Corresponding time for maximum dispersion length occurrence
P	Pressure
P1	Particle 1
P2	Particle 2
r	Particle radius
r_i	Inner radius of sinusoidal channel
r_c	Central radius of sinusoidal channel
r_o	Outer radius of sinusoidal channel
$l_{diff,3D}$	Three dimensional dispersion length
$l_{diff,max}$	Maximum dispersion length difference between particles
ϕ	Level Set Function
ϵ, γ	Numerical stabilization parameters of Level Set Function
ρ	Density
μ	Dynamic viscosity

Chapter 1

Introduction

In 1959, *Richard Feynman* gave a talk called, *There is Plenty of Room at the Bottom*, which inspired scientists to build the foundations of nanotechnology [1]. This talk also established a significant research field, microfluidics, that created new potential research areas in the manner of biology and materials science. In the last couple of years, microfluidic reactors have been a hot topic in research, especially for their promising applications in biotechnology, chemistry and materials science. Microfluidic reactors - or microreactors - are devices that are designed to conduct chemical processes such as material synthesis in an extremely well controlled environment. Generally lateral dimensions of channels in a microreactor are below 1mm and they are capable of maintaining uniform temperature distributions, rapid mixing, or forming droplets of a fluid in another immiscible carrier fluid to perform reactions inside. Further developments in the microreactor technology, will bring new potentials and opportunities for the sake of improvement of automation, control of flow, continuous operation, efficient mixing in multiphase flows, product synthesis, low energy consumption, portability, low manufacturing costs, product quality and reliability [2–4]. Some of the application areas of microreactors are nanoparticle synthesis, nanomaterial growth by heat treatment, polymer coating of microcapsules for drug delivery, DNA detection and analysis as well as biomolecule separation [5–9].

Unique properties of nanoparticles are based on their size, shape and morphology; therefore achieving monodisperse sized nanoparticles is highly desirable to obtain uniform properties within the group of particles. Microfluidic reactors offer a variety of advantages for the synthesis of nanoparticles such as controlled residence time, rapid mixing compared to traditional reactors and fast heating and cooling of the system due to its small size. This high level of control and ability to maintain uniform reaction conditions enable higher throughput and monodispersity [10]. Microfluidic systems based on droplet-based flow reagents are supplied through a single channel, therefore a single stream, before the formation of droplet; that provides high mixing rates after formation of the droplet. [11]. Efficient mixing in microreactors is a key for preparing monodisperse nanoparticles, which provides potential for automating multistep processes like combining analysis, reactions and purification in a single microchip as well as advanced control over size, size distribution and shape [12].

Precise control over reaction conditions and small volumes in microchannels provides various advantages in nanoparticle synthesis and coating over traditional batch-wise methods. In the manner of control over local reaction environment (temperature, reaction rates and concentration), quality of products, uniformity and monodispersity of nanoparticles; synthesis in microreactors have a great advantage over batch-wise synthesis methods [13–17].

In this chapter a brief overview of microreactors will be given and some of the important properties of these devices will be discussed.

1.1 Flow Types in Microreactors

Two types of flow in microchannels are possible: continuous flow and droplet-based flow. In continuous flow, there is only one type of fluid flowing in the channel which takes a parabolic or Pouseuille flow profile. In droplet-based flow, there are two types of immiscible fluids flowing in the channel; where one fluid is carried by the other in the form of droplets.

1.1.1 Continuous Flow

Continuous flow is the most common technique to transport fluids in microchannels. In some applications such as biomedical analysis and biodetection, this method is suitable [18–20]. One of the simplest example, flow in 2D flow simulation of water in microchannel is given in Figure 1.1. (Simulation is performed by using COMSOL Multiphysics.)The equation of flow is given in Equation 1.1.

$$u(y) = \frac{dP}{dx}\frac{y(d-y)}{2\mu} \tag{1.1}$$

Considering fully developed flow or micro-scale flow at low Reynold's number, inertial terms can be neglected, simply we can derive velocity profile in a microchannel; eventually equation of flow will reduce in the form of Stoke's Flow. From Equation 1.1, we can see that flow profile is parabolic and velocity magnitude at walls is zero.

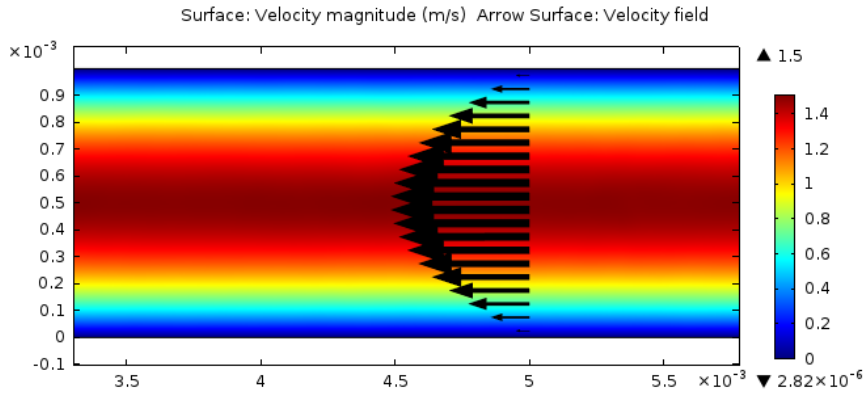

Figure 1.1: Continuous flow simulation in a microchannel

Continuous flow has a parabolic flow profile as can be seen from the figure above. This profile may have disadvantages for some applications. For instance fluid particles near walls move much slower then the ones in the central region of the channel; causing residence time variations inside the channel. For fluids carrying particles, stiction of the substances at the wall may cause instabilities in biodetection [21,22]. On the other hand, in applications such as nanoparticle synthesis,

synthesized nanoparticles may stick to the walls and cause clogging in the channel. Moreover, residence time distributions in nanoparticle synthesis will result in lack of control in reaction times for each sample; resulting in polydispersity.

1.1.2 Droplet-Based Flow

In a droplet-based flow, droplets of a fluid is carried inside an immiscible carrier fluid. This flow type has many advantages over continuous flow due to flow profile obtained. First of all fluid particles circulate inside droplets as they move inside the channel [23], which eliminates the residence time and temperature differences of fluid particles due to the mixing within droplets. Therefore two or more fluids forming a droplet in a channel can be mixed as they move along the channel. This brings the capability of synthesizing nanomaterials by combining and mixing different reagents in precise concentrations within droplets; and also eliminates residence time and temperature distribution among the fluid molecules. As a result much well controlled reactions in microreactors to achieve monodisperse nanoparticles can be performed. Figure 1.2 shows flow of multiple substances in a droplet both theoretically and experimentally.

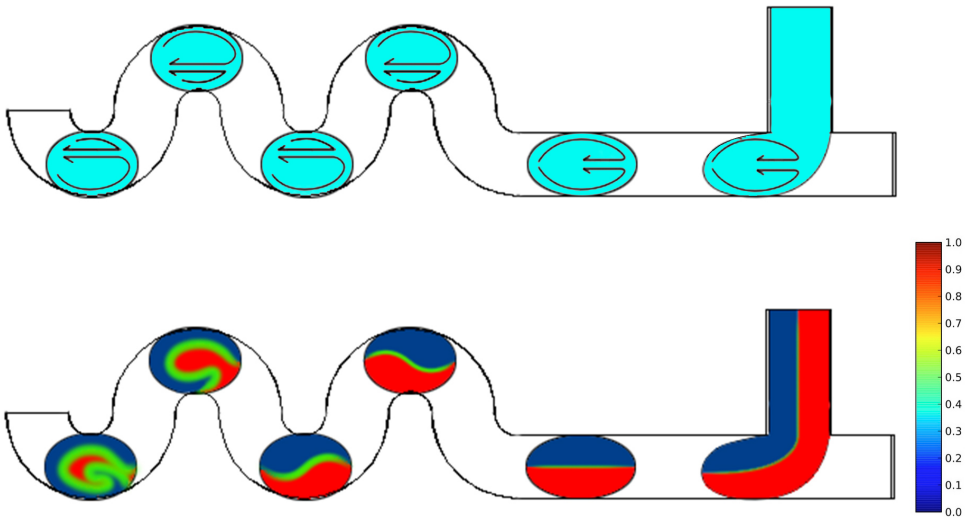

Figure 1.2: Mixing and flow in droplets - schematic explanation

In Figure 1.2, internal circulations in droplets, caused by the shear stress applied

by the wetted walls, are represented with arrows. In this figure droplet motion in a meandering channel is demonstrated as the channel shape increases the mixing rate as will be explained in the next chapter. At junctions internal flow magnitude becomes higher at one side and this creates an internal vortex. When droplet turns to the other direction this vortex changes direction so that mixture in droplet becomes well stirred.

Therefore, we can conclude that droplet-based flow is advantageous over continuous flow due to mixing and control over reaction. The main advantages of droplet-based flow are listed as:

- Precise concentration
- Discrete analysis
- High throughput
- Fast mixing
- Uniform temperature
- Uniform residence time
- No clogging

1.2 Review of Microreactors in Literature

One advantage of micro scale reactors is the fast reaction rates and uniform synthesis results compared to batch-wise methods. Cetin et al. demonstrated the synthesis of chitosan nanoparticles in microchannels with obstacles in microchannels; it was shown by simulations and experimental studies that the synthesis of these types of nanoparticles was faster and more uniform compared to batch synthesis techniques [24]. Erdem et al. demonstrated the TiO_2 synthesis using a droplet-based silicon microreactor with thermally isolated, heated regions. As

a result, monodisperse nanoparticles were obtained. Overall results have shown that synthesis in microchannels and using droplet-based flow provided faster reaction rates and higher quality of nanoparticles as well [25]. Another example similar to the previous study is $FeCl_3$ and $FeCl_2$ synthesis based on circulation inside droplet-based microreactor. As a similar outcome, synthesis of this magnetic nanoparticles provided high quality of uniformity and monodispersity [26]. One other example of nanoparticle synthesis in droplet-based microreactors is the synthesis of magnetic iron oxide (Fe_2O_3). That study has also stated that synthesis in droplet-based platforms is advantageous over bulk synthesis strategies simply for better control of reaction conditions, which provides reduction of nanoparticle size and polydispersity, as well as preservation of physical properties [27]. Shestopalov et al. presented the synthesis of CdSe nanoparticle formed in the scale of miliseconds in a droplet-based platform [28]. Additionally, in the study it has been stated that, multistep reactions including nucleation and growth could be handled in miliseconds due to the advantages of droplet-based flow [28].

According to previous studies, we can conclude that synthesis of nanoparticles in microchannels has a great advantage over batch-wise synthesis methods. Even implementing droplet-based flow would increase performance on microreactors and reaction rates. In this thesis a microreactor system is targeted to synthesize silicon dioxide coatings for quantum dots and conjugated polymer nanoparticles.

1.3 Quantum Dot Nanoparticles

Nowadays, semiconductor materials plays a significant role in various commercial applications such as in LEDs, imaging, biosensing and solar cell devices [29–31]. One of the most unique properties of these materials is holding high energy spectrum at relatively high temperatures. Due to the confinement of electrons, quantum dots stay at discrete energy levels, similar to atoms [32]. Current research on quantum dots consists of single-multiple electron transistor due to electron spin and degrees of freedom [33, 34]. Another application field of quantum dots is quantum computation which allows to do faster computational tasks compared

to traditional computers [35]. In fact, quantum dots exposed to UV light loses their optical properties. Therefore, quantum dots, such as CdSe, InP, ZnP, ZnS and ZNSe are coated with silica (SiO_2) to preserve their properties. Additionally, for buffer stability and to prevent Cd^{+2} leakage; and for providing compatibility with biomolecules, silica shell coating is desired [36–40].

1.4 Conjugated Polymer Nanoparticles (CPNs)

Conjugated polymer nanoparticles (CPN) started to become popular in recent years due to their tunable optic properties (see Figure 1.3), low toxicity in contrast to quantum dots, and photostability. Their low toxicity and organic structure also enable them to be studied for possible applications in biodetection, bioimaging and drug delivery [41–46]. Since their properties depend highly on their size and shape, it is very important to obtain uniform size and shape distribution of these particles. Currently, in literature, they are being synthesized by reprecipitation or miniemulsion methods via conventional methods (batch-wise) [41–46]. However, these methods lack precise control over their size and shape which results in varying properties in the same sample [47]. In this thesis, a microfluidic system is proposed to address the limitations of the conventional techniques in CPN synthesis and the experimental results obtained from this reactor is discussed.

Figure 1.3: Conjugated polymer nanoparticle samples under UV light

1.5 Thesis Overview

Due to the advantages of microfluidics and droplet-based flow as discussed above, this thesis presents a microreactor that has been used for both synthesis of silica nanoparticles and coating of quantum dots with silica layer for the protection of their properties using droplet-based flow. Additionally, a new microreactor was proposed for the synthesis of uniform and monodisperse conjugated polymer nanoparticles.

Chapter 2 presents computational modeling of proposed microreactor and evaluation of mixing performance using spherical nanoparticles, that are placed in droplets inside microchannels. To make a good comparison, position based dispersion length, particle trajectories and particle velocities are compared for different channel structures.

Chapter 3 presents the microreactor designed for silica coating of nanoparticles. Fabrication of the device using mechanical machining combined with soft-lithography method and photolithography method are explained. Experimental results of silica synthesis within the microreactor is shown. The design of the microfluidic device was completed according to the results of simulations discussed in Chapter 2. Limitations of mechanical machining technique on droplet formation within the microreactor was discussed.

Chapter 4 presents the microreactor designed for the synthesis of conjugated polymer nanoparticles. Fabrication of the device using photolithography and soft-lithography techniques was discussed. Experimental results of conjugated polymer nanoparticle synthesis within the microreactor were presented. Effects of residence time in channels and flow type are discussed and results obtained from the microreactor were compared to the results obtained by batch-wise synthesis.

Chapter 5 summarizes and highlights the important outcomes and findings of this work and proposes possible future works.

Chapter 2

Design of the Microfluidic Device

2.1 Design Criteria

Design of a microreactor with capability to rapidly mix the reagents required for the synthesis is the focus of this chapter. Mixing rate of multiple ingredients for both silica coating and polymer nanoparticle synthesis should be high enough to prevent agglomeration and provide fast reaction rates. As it is discussed briefly in Chapter 1, droplet based flow provides better mixing performance compared to continuous flow. To generate droplets, there are various method such as flow focusing and utilizing a t-junction. Since flow focusing device is used for larger geometries of microfluidic devices and for some critical fluids, we have implemented multiple t-junctions in our device. Additionally, since multiple ingredients are required for the synthesis, 3 t-junctions are implemented for each device. Moreover, residence time is another issue that we need to consider for the synthesis rate. To do that, 3 outlets for obtaining 3 different residence times were utilized. By this way, it will be possible to make a systematic study of the effect of residence time on coating thickness. Additionally, to increase internal circulations of droplets, sinusoidal microchannels are implemented after the formation section. In fact, channel cross-section and sinusoidal section geometry is still an issue whether smaller or bigger geometry is better for high mixing rates. In the next

section, mixing performance in droplet based motion in sinusoidal microchannels for different geometries is analyzed.

2.2 Numerical Analysis of Mixing Performance in Sinusoidal Microchannels

Mixing in microscale is limited to dispersion length and this makes it difficult to achieve fast and effective mixing in continuous flow microfluidics. Utilizing sinusoidal -or meandering- microchannel geometry to mix multiple substances is one of the most common techniques in microfluidic devices [48–50]. Another method to improve mixing in continuous flow is chaotic mixing. In a steady chaotic flow, fluid movement in different directions increases the mixing effect [18, 51]. On the other hand droplet based microfluidic systems have several advantages over continuous flow systems due to the circulating flow profile inside droplets as opposed to parabolic flow profile; which increases the diffusion and the speed of mixing [52–54].

Experimental investigation of mixing performance of multiple reagents inside droplets using dyes proved that it is a rapid method for mixing without dispersion [55]. Another study on mixing includes chaotic advection introduced by a variety of winding geometries for folding, stretching and reorienting bulk fluid which accelerates mixing rate of the high Peclet number systems [56]. Moreover, some studies are conducted for real time monitoring of droplet based mixing in microchannels using Fluorescence Lifetime Imaging [52, 57].

Even though it was shown experimentally that the mixing in droplets are faster compared to continuous flow, it is necessary to understand how each parameter (channel dimensions, size of droplets, position based dispersion length, etc.) affect the mixing performance. Some of the previous numerical work on mixing includes a study on chaotic mixing inside rotating droplets [58]; mixing performance in droplets with induced steady and unsteady flow inside [59]. Additionally, droplet

motion over obstacles and spacing of droplets and generation algorithms have been studied by different research groups to understand the physics of droplet motion in the computational manner [60,61]. Previous computational fluid dynamics (CFD) simulations are based on either Lattice Boltzmann Method [62], Boundary Element Method [63] or Finite Elements with Level Set Method [64–66]. Finite Element Method combined with Level Set Method has been used more frequently among the other numerical approaches.

The objective of this study is to understand the effect of geometry of the channel on the mixing performance in a droplet-based system using numerical techniques. Utilizing finite element analysis, droplet formation is simulated and flow profile inside droplets are visualized via particle tracking. To understand the mixing performance, different parameters such as dispersion length, particle trajectories in vertical direction and particle velocities inside the droplets are calculated. This study is iterated for different channel cross-sections and mixing zone profiles.

2.2.1 Theory & Modeling

Among the various droplet formation methods, one of the most common methods of forming droplets in microchannels is to use a T-junction. In a T-junction, droplets are generated by shear stress applied by the immiscible carrier fluid. In order to increase the efficiency of mixing, sinusoidal channel profile is used so that distortion on the droplet surface will provide additional reduction of dispersion length inside the droplet; eventually reducing the time required for mixing.

In order to simulate droplet motion, Level Set Method; which is an iterative, numerical technique to track interfaces and shapes, is used. By combining governing equations, momentum transport equation and level set method, one can simulate multiphase fluid motion considering fluid interface by using finite elements. Equations 2.1, 2.2, 2.3 [67] represent Reynolds momentum transport, continuity and level set equations respectively.

$$\rho\frac{\partial u}{\partial t} + \rho(u.\bigtriangledown)u = \bigtriangledown.(-pI + \mu(\bigtriangledown u + (\bigtriangledown u)^T)) + F_{st} \tag{2.1}$$

$$\bigtriangledown .u = 0 \tag{2.2}$$

$$\frac{\partial \phi}{\partial t} + u. \bigtriangledown \phi = \gamma \bigtriangledown .(-\phi(1-\phi)\frac{\bigtriangledown \phi}{|\bigtriangledown \phi|}) + \epsilon \bigtriangledown \phi \tag{2.3}$$

where, ρ is density, u is velocity, t is time, μ is dynamic viscosity, P is pressure, F_{st} is the surface tension force, ϕ is level set function, γ and ϵ are numerical stabilization parameters. Level set function will determine the density and viscosity at the interface between the droplet and the carrier fluid by using equations 2.4 and 2.5.

$$\rho = \rho_1(1-\phi) + \rho_2\phi \tag{2.4}$$

$$\mu = \mu_1(1-\phi) + \mu_2\phi \tag{2.5}$$

Equations given above were implemented in Comsol Multiphysics$^{c}ircledR$ to simulate droplet generation and particle motion. To test mixing in microchannels, 17 identical 90° arcs were added after droplet formation zone to form the sinusoidal mixing channel. For all simulations, number of arcs was kept constant. The schematic of the computational domain of the simulation is shown in Figure 2.1.

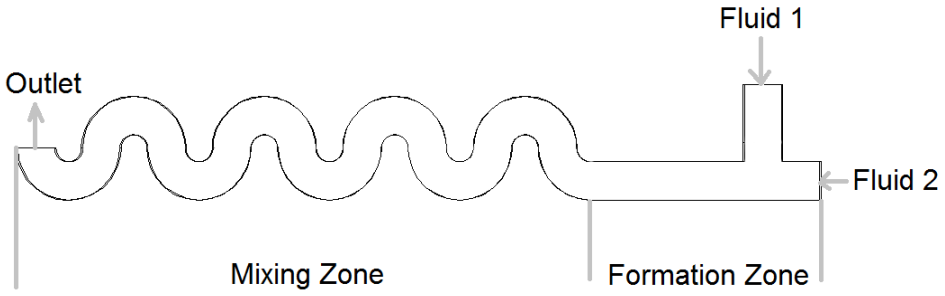

Figure 2.1: Schematic of the computational domain of the simulation

As it is seen in Figure 2.1, the domain has two separate sections that are the mixing zone and the formation zone. In the formation zone droplets were generated at the T-junction. In the mixing zone, the mixing performance of sinusoidal channels according to different parameters was analyzed. Boundary conditions

were chosen as 'wetted wall boundary condition' at the channel walls and 'zero pressure boundary condition' at the exit. Flow rates were defined at the inlets. In order to reduce the computational expense of the simulation, only one half of the domain was solved since the problem is symmetric in y-direction. As a result, formation and circulation of half droplet was simulated. Once the simulation was completed, results were mirrored in y-direction to visualize the whole domain. Flow parameters of the simulations are given in Table 2.1.

Table 2.1: Simulation parameters

Fluid 1	Density	1000 kg/m^3
	Viscosity	1.95×10^{-3} Pa.s
	Flow Rate	1.11 m^3/s
Fluid 2	Density	1000 kg/m^3
	Viscosity	6.71×10^{-3} Pa.s
	Flow Rate	2.22 m^3/s
Droplet	Contact Angle(θ)	135°
	Slip Length (β)	0.5 mm
	F_{st}	0.005 N/m
Particle	Density	1000 kg/m^3
	Diameter	0.5 nm

In order to analyze motion within the droplet, multiple spherical nanoparticles were introduced in flow so that tracing their motion would give an idea about the efficiency of the mixing. Particle movement inside droplets represents the mixing rate in the flow. Motion of a spherical particle in fluid medium with low Reynolds Number flow, is formulated as [68];

$$\mathbf{F}_{\text{drag}} = 6\pi\mu r\mathbf{u}_{\text{rel}} \tag{2.6}$$

Position, velocity and acceleration of each particle is calculated from following equations using Equation 2.6:

$$x(t) = (\frac{\mathbf{F}_{\text{drag}}}{m})t^2 + v_o t + x_o \tag{2.7}$$

$$a(t) = \frac{\mathbf{F}_{\text{drag}}}{\text{m}} \tag{2.8}$$

$$v(t) = \int \frac{\mathbf{F}_{\text{drag}}}{\text{m}} dt \tag{2.9}$$

Additionally, to determine the mixing performance in microchannels, different parameters were used. First one was the dispersion length which is denoted in the following equation [69]:

$$l^2_{\text{diff,3D}} =< x^2 + y^2 + z^2 > \tag{2.10}$$

Dispersion length, or in other words mixing length, is defined as the representative of the Peclet number of a numerical scheme, where dispersion of a bulk fluid is taken into consideration. Different from other mixing terms like diffusion, dispersion length, which is representative of diffusion and convection of the fluid, is measured in terms of the characteristic geometric length [70, 71]. This equation was used to determine the particle dispersion length with respect to its initial release position in Cartesian coordinates (x,y,z). In each case, particles were released from the same initial position. For higher mixing performance, wider difference between two dispersion lengths of different particles was expected. Oppositely, if there was not hydraulic mixing inside the droplet, dispersion length difference between two particles was expected not to change through the simulation.

Particle velocity and displacement in vertical direction are the other parameters that determine mixing performance. Simulations were repeated for different dimensions of the microchannel both in mixing zone geometry and channel geometry. Those geometrical variations; inner(r_i), central(r_C) and outer(r_O) radius of mixing zone for different channel cross section, are given in Table 2.2.

Table 2.2: Mixing zone dimensions for different cases

	100μm×100μm			120μm×120μm		
Case	1	2	3	4	5	6
r_i(mm)	0.02	0.05	0.07	0.02	0.05	0.07
r_C(mm)	0.07	0.10	0.12	0.08	0.11	0.13
r_O(mm)	0.12	0.15	0.17	0.14	0.17	0.19

2.2.2 Results and Discussion

To determine the fluid flow and particle movement, Comsol Multiphysics$^{c}ircledR$, which is a finite element analysis software, is used. Since fluid flow equation is independent of particle movement in flow field; first Level Set, Reynolds Momentum Transport and Governing Equations were solved, later particle movement was solved. Fluid was assumed to be incompressible and Newtonian.

In order to check the accuracy of the model, effective droplet diameter and volume were compared with numerical and experimental study in the literature [72]. Additionally, whether there is phase leakage between droplets and the carrier fluid were checked. Results of this comparison is shown in Table 2.3.

Table 2.3: Comparison of model accuracy using effective droplet diameter with literature.

	Simulation	Experiment (lit)	Simulation (lit)
$d_{effective}$(μm)	116.5	106.2	101.2
% Error		8.70	13.06

As it is seen from Table 2.3, our model result matches with the experimental and other simulation results from the literature. Reason of this error difference between literature and our simulations is due to the difference of the applied numerical methods. However, showing only droplet diameter is not sufficient for validating the reliability of the results. Phase leakage is also an issue in Level Set Method, where mass of fluids are not conserved due to the leakage from one liquid to the other. Moreover, high contrast in density and viscosity increases the possibility of leakage. On the other hand, in literature it was denoted that

for two liquid phases, phase leakage is a minor problem [73–75]. Nevertheless, we calculated the phase leakage as well as the effective droplet volume change in every time step to show that phase leakage is not very significant in our problem.

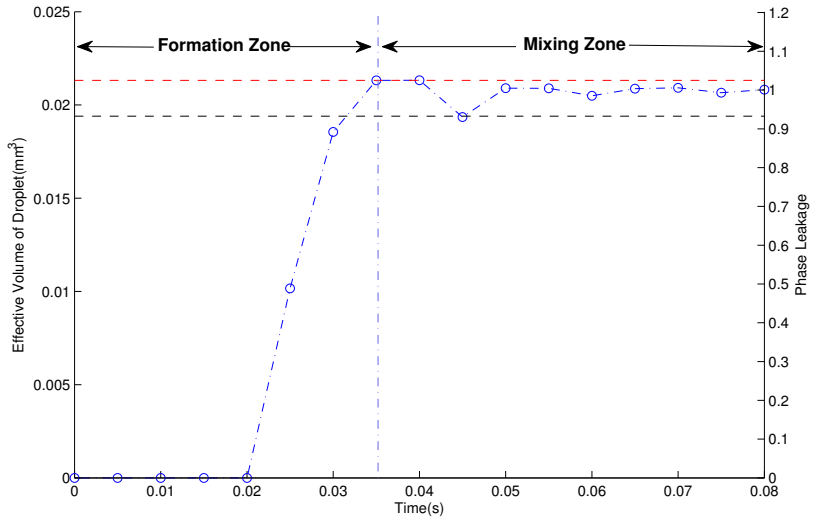

Figure 2.2: Volume of the droplet and phase leakage calculation in formation and leakage zones. Volume of the droplet was calculated by $V = h4\pi/3(d_{effective}/2)^2$. Phase leakage was calculated by Comsol Multiphysics®. The mesh domain consists of 222817 domain elements, 29665 boundary elements, 2209 edge elements and number of degrees of freedom is 1349253.

From Figure 2.2, we can see that the effective volume of the droplet is increasing in the first 0.035 seconds, which is the time during which the droplet is formed. After the droplet is formed, it enters the mixing zone and it can be seen that the volume of the droplet is steady and phase leakage does not affect the volume of the droplets significantly. For a similar leakage case discussed in [73], this was considered as a minor leakage. Therefore, in our simulations phase re-injection was not implemented and we can state that the simulation results are consistent and reliable.

In this study, 6 different cases with varying channel dimensions were tested. These cases are listed in Table 2. In each case, 2 particles were released from the same location in the droplet. Mixing performance in different channel dimensions were analyzed. Droplet motion and differentiation of one fluid from another was done

by using isosurface and volume fraction along with constant density in the volume space. Visualization of droplet motion shall be seen in Figure 2.3 and Figure 2.4.

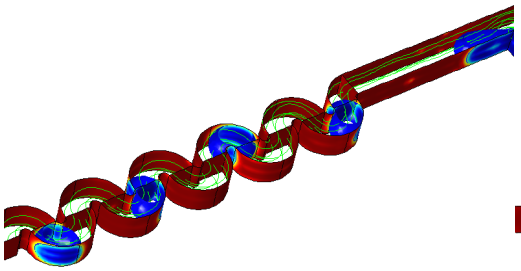

Figure 2.3: Droplet formation in microchannels using isosurface

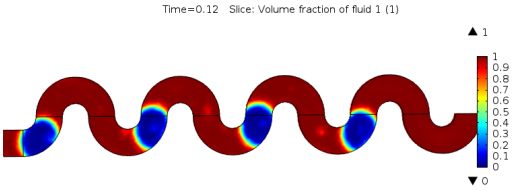

Figure 2.4: Volume fractions of the fluids

As it is seen in Figure 2.3, droplets, indicated in blue color, are successfully formed, carried in the carrier fluid and circulated in the sinusoidal channel without any dissipation from droplet to carrier fluid. Moreover, green lines in the microchannel indicate streamlines of the flow. Volume fractions of Fluid 1 and Fluid 2 shall be seen in Figure 2.4. Green contour around the droplet indicates the interface around the droplet.

The results of the first set of simulations, particle displacement, velocity profile and dispersion length of first three cases are represented in Figures 2.5, 2.6 and 2.7.

According to results in Figure 2.5, each particle circulates in the sinusoidal channel as it was expected. Due to the geometrical difference in each case, highest and lowest particle displacement in vertical direction varies. The irregularities in the formation zone are due to the initial formation of the droplet. This is effective in distinguishing two different particles which were released very close to each other. At t=0.03s, formation ends and droplet begins to cycle in the straight part of the channel. At t=0.45, it enters the mixing channel with sinusoidal shape. According to these results we observed that the vertical displacement between each particle varies with time. Furthermore, in channels with larger central radius, vertical displacement of two different particles have similar trajectories which is not desired for mixing. As the channels scale down, trajectory variation between

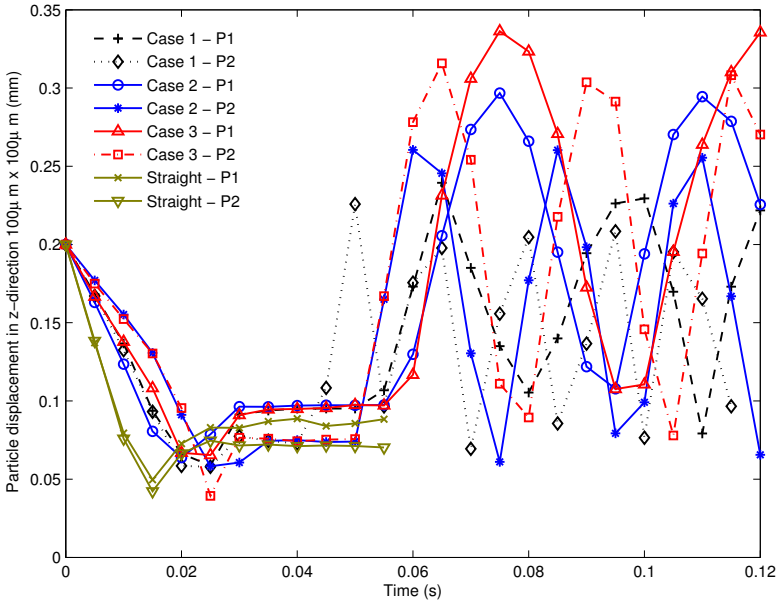

Figure 2.5: Displacement of particles at 100μm$\times 100\mu$m channel cross-section and comparison with straight channel profile.

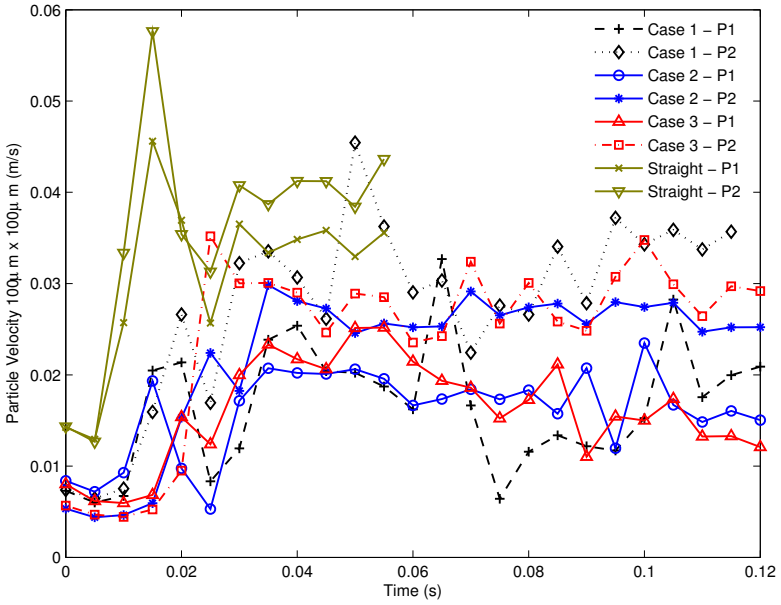

Figure 2.6: Velocitiy of particles at 100μm$\times 100\mu$m channel cross-section and comparison with straight channel profile.

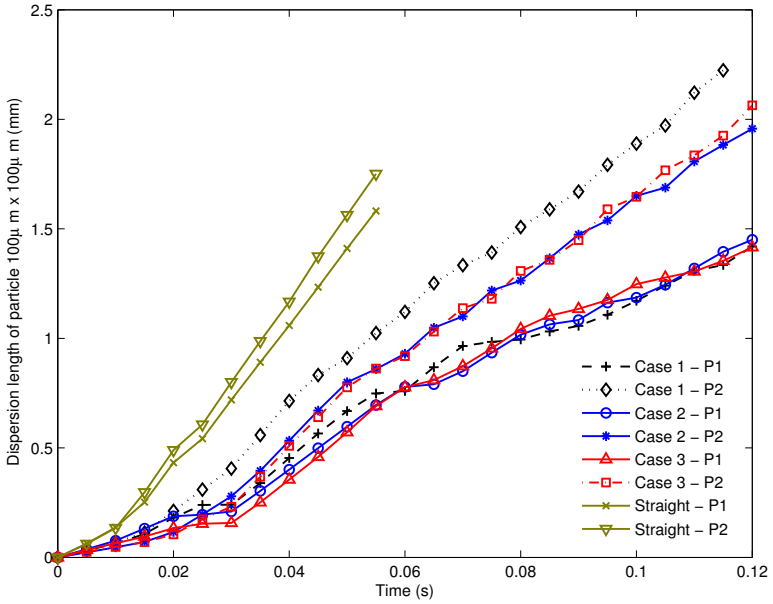

Figure 2.7: Dispersion lengths of particles at 100μm$\times 100\mu$m channel cross-section and comparison with straight channel profile.

two particles released at the same location increases, which validates the experimental results in literature that show faster mixing in sinusoidal channels with smaller central radius [76]. In straight channels particle path in droplets does not change significantly in vertical direction which proves the necessity of sinusoidal shape to increase the mixing rate.

When the velocity profiles in Figure 2.6 were checked, it can be seen that, the velocity of particles in straight channels do not change much since there is not any collusion of droplet to side walls or meandering parts of the microchannel. However, in sinusoidal channel profiles there is a significant velocity variation between particles. Especially in channels with smaller central radius, velocity variation is larger compared to the ones with larger radius. This variation has an important role in hydrodynamic mixing since velocity variation inside the droplet certifies velocity profile variation inside the droplet as indicated in [77]. That is to say, having more fluctuation in the magnitude of the velocity improves the mixing performance. Therefore, having greater variance between particle velocities inside droplets is more likely in channels with smaller central radius, providing better

mixing compared to channels with larger central radius.

Dispersion length variation is the other crucial parameter for determining the mixing performance. As it is explained in the theory part of this article, distance between particles inside the same droplet will indicate the mixing rate. Greater dispersion length variation between particles will result in better mixing performance. Figure 2.7 shows that the dispersion lengths between two particles does not change significantly in channels with 100μm by 100μm cross section. Likely in Figure 2.5, dispersion length of particles moving in the straight microchannel does not change. Therefore change in dispersion length in straight microchannel is only due to regular motion of the droplet which is not sufficient for faster mixing rates. On the other hand, in sinusoidal channels, dispersion length variation increases in each time step since wave like motion of droplets provides a non-uniform velocity profile inside droplets. So that, location of each particle changes significantly in each time step. Moreover, variation between dispersion length between two particles increases as the curvature radius of meandering channel decreases; which rapids up the mixing inside the droplet. This is also due to the higher non-uniformity of the velocity profile inside the droplets in channels with smaller central radius.

By looking at the results, it can be concluded that channels with smaller central radius show better performance compared to channels with larger central radius based on three findings; i) change in vertical displacement in smaller radius channels is more frequent compared to channels with larger radius; ii) there are more velocity peaks and variations through mixing process in channels with smaller radius; iii) dispersion length difference between two particles is larger compared to channels with larger radius. In the next section, same parameters will be used to simulate mixing performance where cross-sectional area of microchannel will be increased from 100μm$\times$100μm to 120μm$\times$120μm. Figure 2.8, 2.9, 2.10 represent particle displacements in vertical direction, velocity variation and dispersion length of particles in this channel profile.

According to results in Figure 2.8, particle motion shows similarities as in the case of 100μm$\times$100μm channel profile (Figure 2.5). Similarly, particle displacements

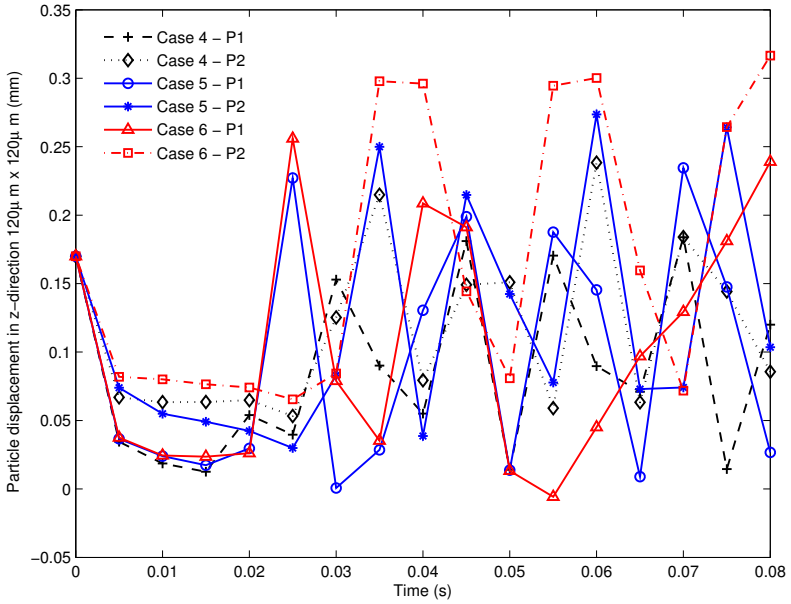

Figure 2.8: Displacement of particles at 120μm×120μm channel profiles.

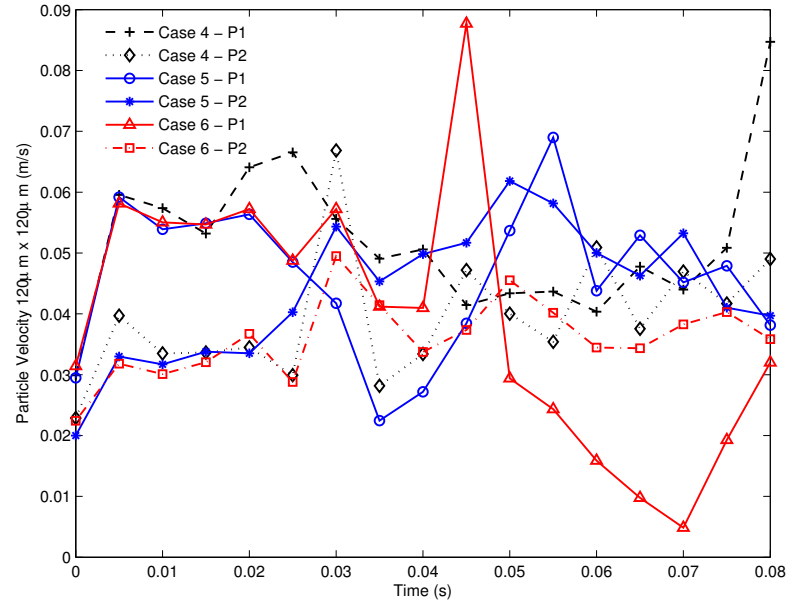

Figure 2.9: Velocity of particles at 120μm×120μm channel profiles.

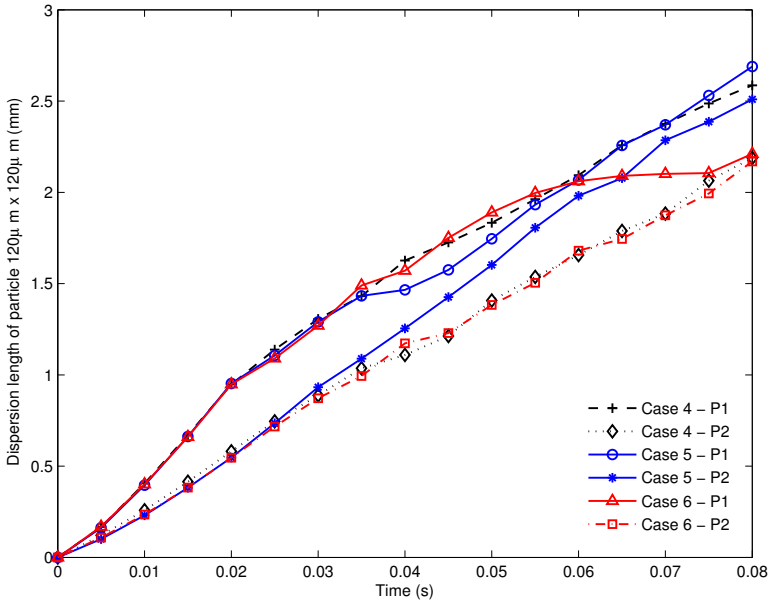

Figure 2.10: Dispersion length of particles at 120μm×120μm channel profiles.

in vertical direction differ faster compared to channels with wider central radius. In fact, in 100μm×100μm channel profiles, particles reach mixed conditions in a shorter time. If we compare Figure 2.7 and Figure 2.8, 100μm×100μm channel profile particles of Case 1 reaches to opposite locations in t = 0.08s. In fact, in 120μm×120μm channels of Case 4, particle positions do not change frequently during the simulation time which is undesired for mixing inside the droplets.

As seen in Figure 2.9, variation in particle velocities is different for different dimensions of channels. In channels with a larger cross-sectional area, velocity values of particles are larger compared to channels with a smaller cross-sectional area.

Dispersion length variation between two particles (P1, P2) for different cases is shown in Figure 2.10. As it is expected, smaller central radius channel profile provides more dispersion length variation between two particles. Additionally, for channels with larger radius, dispersion length variation decreases. However cases 5 and 6 does not have much of a difference. Unlike Figure 2.7, dispersion length variation in cases 2 and 3 are visually more different than the cases in

wider channel geometry. Due to that reason, we can understand that in channels with larger radius, increase in cross-sectional area decreases the mixing performance inside droplets. Furthermore, dispersion length difference between cases 1 and 4 shows a significant variance. If we check the dispersion length difference at t=0.08s, for smaller cross-sectional geometry, dispersion length difference is larger than the case for larger cross-sectional area. Therefore it can be concluded that smaller cross-sectional geometries are more suitable for faster mixing rates. Overall, maximum dispersion length percent and corresponding time for each case is given in Table 2.4 as a summary of these results.

Table 2.4: Maximum dispersion length difference percentage for each case.

$l_{diff,max}$ = 0.89 mm

Case #	1	2	3	4	5	6	Straight
$l_{diff,max}$ (%)	100	57.10	72.96	58.21	45.78	58.68	19.02
$t_{corr.}$(s)	0.12	0.12	0.12	0.040	0.020	0.045	0.055

According to Table 2.4, case 1 reaches to maximum dispersion length towards the end of the simulation whereas for cases 4, 5 and 6, maximum dispersion length is not reached at the end of the simulation; which is not very efficient. Moreover, case 1 provides five times greater dispersion length difference between particles than the straight microchannels, which proves that sinusoidal channels are better for mixing.

2.3 Final Device Design

In this section, finite element analysis used for modeling fluid flow and droplet formation inside microchannels by tracking interface between heterogeneous two fluids and multiple particle trajectories inside a droplet is explained. The solutions of multiphase fluid flow and particle trajectories were coupled to each other so that drag on every single particle changes in every time step. To solve fluid

motion in multiphase flow, Level-Set Method was used. Parametric study was repeated for six different channel dimensions including change in channel curvature and cross-sectional area. These results were compared with mixing in droplets inside a straight microchannel. Additionally, tracking of multiple particles inside a droplet was performed to simulate the circulating flow profile inside the droplets. Based on the calculation of the diffusion length, particle trajectories and velocities inside droplets; it was observed that having smaller channel geometries increases the mixing performance inside the droplet which shows that this form of fluid flow is very suitable for performing chemical reactions inside droplets as it will occur faster. Moreover, narrower and meandering microchannels showed 5 and 2 times better diffusion length difference performance compared to the straight and wider microchannels respectively.

Based on the simulation results it was concluded that the cross section of the sinusoidal channel should be as small as possible and the microfluidic device was designed accordingly. A microfluidic device that can mix four reagents inside a droplet was designed to increase the flexibility in the usage of reagents. These reagents meet at a junction where the carrier fluid will break them into droplets as simulated. CAD drawing of the design, made by using Solidworks, is shown in Figure 3.1. Additionally, dimensions of the microfluidic device are given in Table 2.5.

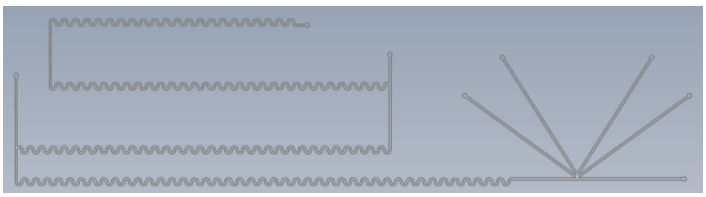

Figure 2.11: CAD drawing of the silica coating microfluidic device

Table 2.5: Dimensions of the silica coating microfluidic device

Device area	70 mm × 21 mm
Total channel length	237 mm
Channel cross-section	200 μm × 200 μm
r_i	0.17 mm
r_o	0.37 mm

Chapter 3

Silica Synthesis & Coating

3.1 Fabrication of the Microfluidic Device

Microfluidic devices shall be manufactured using various methods and materials. One common method is to fabricate a mold and later cast a polymer on this mold to obtain the microsystem. Two main methods for obtaining a mold are micromachining and microfabrication in clean room. In micromachining, mold is manufactured using milling operation, then soft-lithography technique is applied to form microchannels. Oppositely in microfabrication technique, channels are formed by etching. Micromachining though may result in rougher surface [78]. On the other hand, microfabrication provides a better surface finish [79–81]. Apart from that, micromachining requires less work load due to simplicity of processes. As mold material SU-8 photoresist, silicon, plexi-glass and metal based materials such as brass, stainless steel were commonly used in previous works [82–84]. For the sake of droplet formation, fabrication of the mold plays a crucial role at this point since surface quality directly affects the quality of the resultant microreactor. According to the simulation results, we understood that meandering channel cross section should be as small as possible, which is an other limitation for fabrication technique.

3.1.1 Mechanical Machining Technique

In this technique, Fabrication of microreactors mold was done in the facilities of Bilkent University Micro System Design and Manufacturing Center. Using computer aided manufacturing (CAD) programs and machining processes, plexi-glass mold was manufactured. In the CAD program, adaptive feed rate control and interpass cleaning were used. With less than 1μm run out option, DECKEL MAHO-HSC55 milling machine with HES510-HSKA63 spindle head was used. Using KISTLER-9256C1 mini-dynamometer allowed us to control machining in z-direction with better accuracy. Minimum channel dimensions were determined according to the machining limitations. CAD drawing of the mold, made by using Solidworks, is given in Figure 3.1. Additionally, dimensions of the microreactor and machining parameters were given in Table 3.1 and Table 3.2 respectively. Moreover, machining steps of the plexi-glass mold is given in following flow chart. Machining time took around 5 hours.

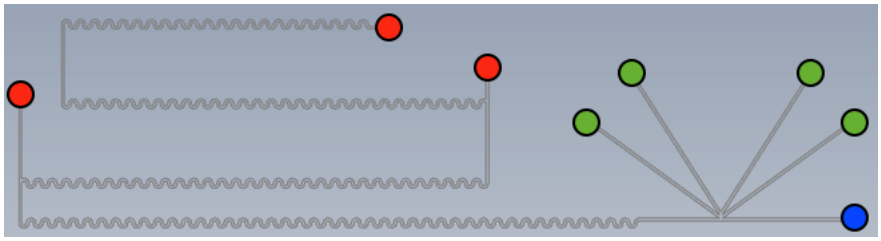

Figure 3.1: CAD drawing of silica coating microfluidic device. Green marks indicate transporting fluids, blue mark indicates carrier fluid and red marks indicate outlets to analyze residence distribution time.

Table 3.1: Dimensions of the microfluidic device

Device area	70 mm $\times$ 21 mm
Total channel length	237 mm
Channel cross-section	200 μm $\times$ 200 μm
r_i	0.17 mm
r_o	0.37 mm

1. Face milling operation was applied to the rough material with a tool diameter of 2mm. Flatness of the stock surface was ensured with end milling operation.

2. To generate mold cavity, pocket milling operation was applied.

3. To generate microchannels, contour milling was applied. Diameter of the tool is 0.34 mm.

Table 3.2: Machining parameters of the microfluidic device

Material of the tool	Tungsten carbide steel, HSS
Number of teeth	2
Diameter of the tool	0.34 mm
Spindle speed	15000 rpm (Maximum)
Material of the mold	Poly(methyl methacrylate) - Plexiglass

After the fabrication of the mold, polydimethyl siloxane (PDMS) was poured into the mold. PDMS was cured for 60 minutes at 80°C. Afterwards, PDMS was peeled off from the mold and was exposed to oxygen plasma for 30 seconds along with the glass slide to be bonded. Finally, microreactor and glass slide was bonded. Full fabrication steps are available in Appendix B. Manufactured PDMS based microreactor shall be seen in Figure 3.2. Additionally, microscope images of the 4 inlet t-junction of the microreactor is shown in Figure 3.3.

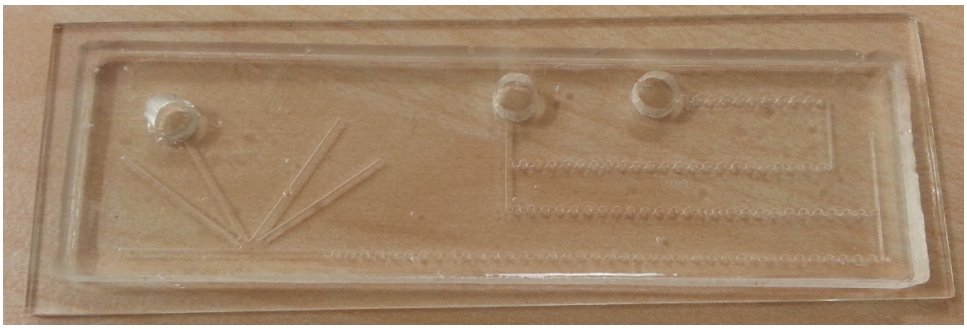

Figure 3.2: PDMS based microreactor manufactured from soft lithography technique

From the microscope images, it has been seen that 4 inlet T-junction was highly effected from tool diameter as it is seen in Figure 3.3. There are clearly visible fillets around the junctions, which is problematic for droplet formation. Nevertheless, using an alternative scheme, microreactor was used for silica coating.

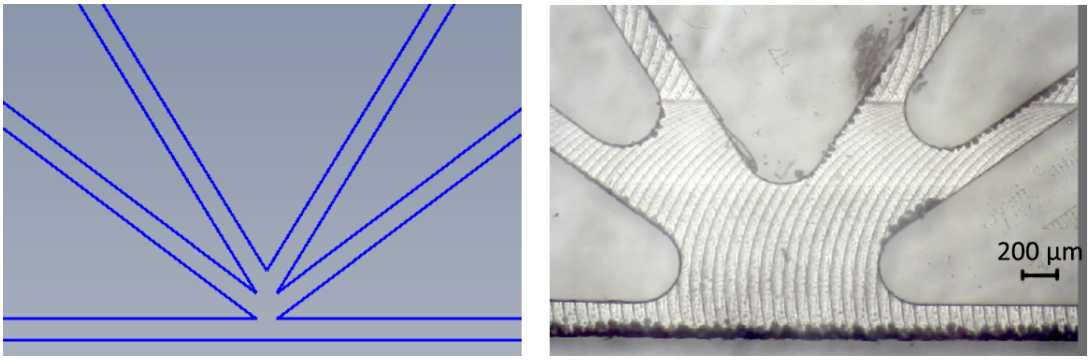

Figure 3.3: Effect of the tool diameter on junctions - comparison with CAD drawing and microscope image of the fabricated device

3.1.2 Photolithography Technique

Due to the effect of tool diameter on junctions, microfabrication technique was chosen to manufacture the new microreactor; this technique provides better surface quality and more precise junction point structures. Accordingly, new design shall be seen in Figure 3.4.

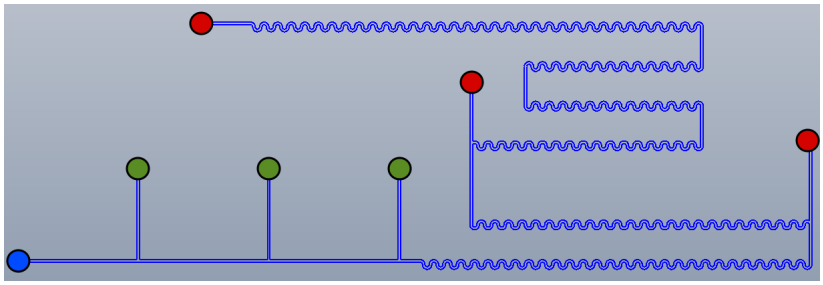

Figure 3.4: CAD Drawing of new design of Silica Microreactor. Green marks indicate transporting fluids, blue mark indicates carrier fluid and red marks indicate outlets to analyze residence distribution time

In the new design, location of each inlet was changed. After formation of droplet, additional reagents was implemented from following junctions. Flow chart of photolithography manufacturing process of silica coating microreactor is given in Figure 3.5. Thickness and photoresist dependent parameters were acquired from Clariant company reciperec1. Since the mask also consists of silica and conjugated polymer microreactor (Appendix C), both devices was placed on a single silicon wafer.

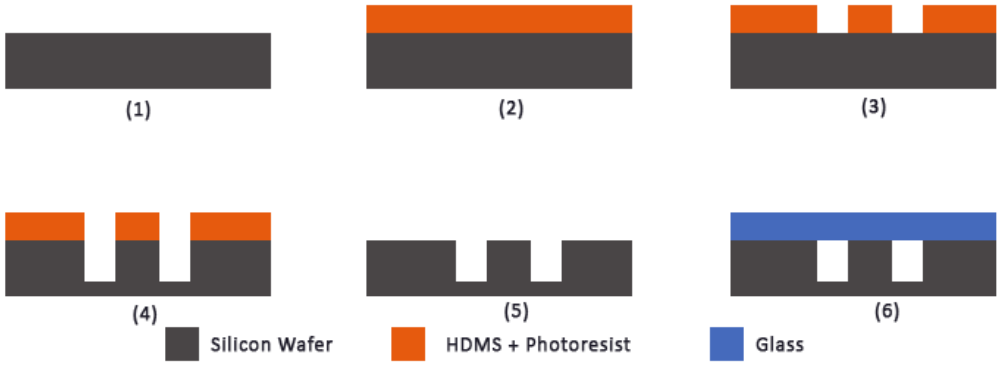

Figure 3.5: Fabrication steps of silica coating microreactor using photolithography technique

1. Initially, Si wafer was rinsed with Acetone, Isopropanol and D. I. water respectively. Then, wafer was dried with Blow Dry until no water droplet left on both surfaces.

2. Later on, wafer was placed in the oven for 7 minutes at 110°C to remove remaining water particles and moisture on the surface.

3. Then, cleaned wafer was hold in the ambient for 4 minutes to cool down the wafer.

4. Cleaned substrate was coated with HDMS and AZ 5462 (positive photoresist). Spinning time, velocity and acceleration for both chemicals are given respectively: v_{HDMS} = 5000 rpm, a_{HDMS} = 2000rpm/s, t_{HDMS} = 40s; v_{PR} = 4000 rpm, a_{PR} = 2000rpm/s, t_{PR} = 40s. Resultant HDMS and PR thickness was 1.4 μm. The purpose of coating substrate with HDMS is to provide better stiction of photoresist to the substrate.

5. After the spinning process, wafer was baked on a hot plate for 50 seconds at 110°C (Pre-bake). To have a gradual increase in temperature on the substrate at longer bake times, substrate could be heated at 65°C for a shorter time, depending on the photoresist thickness.

6. Afterwards, wafer was exposed to UV light under 200 mJ/cm^2 power with proximity. Separation distance was selected as 200μm, proximity was

500μm, mask thickness was 2.3μm, substrate thickness for a 4 inch wafer was 500μm and resist thickness was 6μm.

7. Later on, exposed wafer was held on the hot plate for another 50 seconds at 110°C (Post-bake). (50 seconds should not be be exceeded in order to preventcrackings on exposed photoresist.)

8. Baked wafer was held at room temperature for 4 minutes to cool down. If this cool down process was not done, there would be cracks in the microscopic level on the photoresist.

9. After the cooling process, photoresist was developed in AZ 400K developer for 50 seconds. Developer should be diluted with D. I. water with 1:4 ratio (more water concentrated) [85]. Exceeding development time will cause non-uniformity on photoresist on the wafer surface, which is called as over-developing.

10. Wafer was rinsed with isopropanol and water and blow dried with N_2. (At this step, acetone should not be used, otherwise all photoresist layer will be damaged and stripped of due to acetone.)

11. Silicon substrate was etched by deep reactive ion etching (DRIE) until a depth of 200μm(channel depth) was obtained. The reason of using DRIE instead of DRIE was due to advantage over high aspect ratio, selectivity and capability of reaching nearly vertical side walls [86, 87]. This process, especially for etching Silicon wafer is called *Bosch Process*, that was invented by Robert Bosch [88]. Etching process took around 4 hours. Parameters that were used for Bosch Process, DRIE are listed in Table 3.3.

12. Photoresist layer was removed using acetone once the etch was over. Removing process was done by placing substrate in a beaker filled with acetone in an ultrasonic bath. Process took around 10 minutes.

13. Remaining Si substrate was bonded to glass wafer using anodic bonding at METU MEMS Facilities.

14. Inlets of channels was drilled on the glass using micromilling technique with following parameters: 6000 rpm spinning speed, 20 mm/min feed rate. Poly crystalline diamond (PCD) drill was manufactured using micro electro-discharge machining. Diameter of the drill is 0.7 mm. Drilling of a single hole took around 1 minute.

Table 3.3: Bosch process parameters

	Passivation	Etching
Cycle Time	7 s	10 s
Pressure	20 mT	35 mT
C_4F_8 Flow	70 sccm	-
SF_6 Flow	-	80 sccm
O_2 Flow	-	5 sccm
Ar Flow	-	-
Coil Power	400 W	400 W
Bias Power	-	13W
Bias Frequency	-	13.56 MHz
Ar Flow	-	-
Chinner Temperature	20°C	20 °C
Heater Temperature	-	45 °C
Platen Matching	Load, 35, Tune 50	Load, 35, Tune 50
Coil matching	Load, 40, Tune 60	Load, 40, Tune 50

Finally, surface and height profiles of fabricated device were visualized using scanning electron microscope (SEM) and laser microscope images and represented in Figure 3.6,3.7,3.8 and 3.9. Additionally, laser image of 3 inlet junction and silicon wafer microfluidic device is shown in Figure 3.10 Figure 3.11.

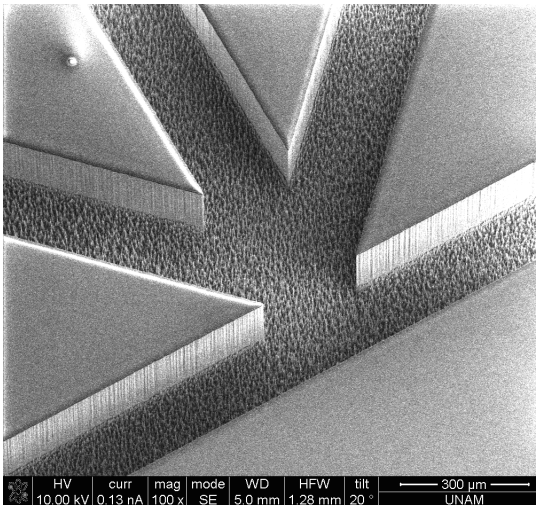

Figure 3.6: SEM image of the 3 inlet t-junction

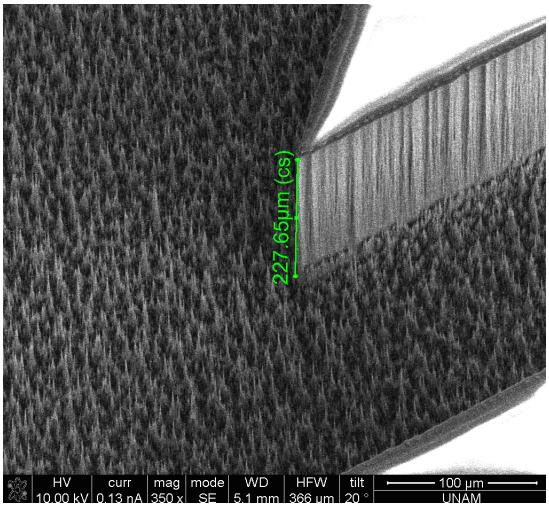

Figure 3.7: SEM image and height profile of the edge of 3 inlet t-junction

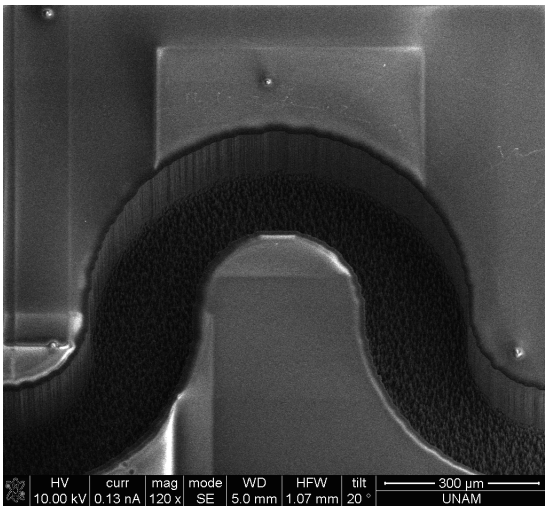

Figure 3.8: SEM image of sinusoidal section

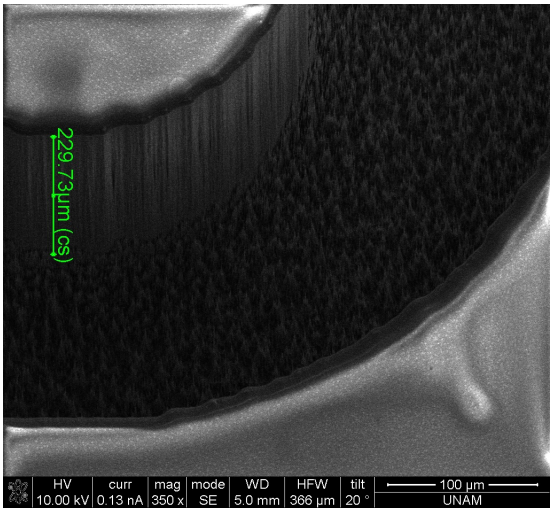

Figure 3.9: SEM image and height profile of sinusoidal section

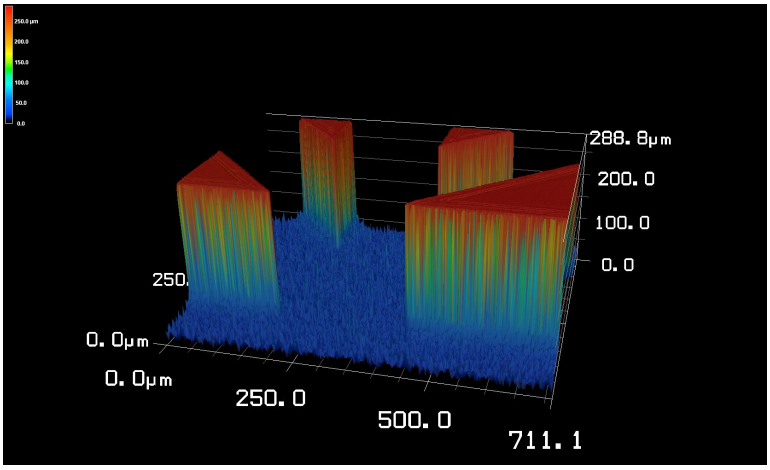

Figure 3.10: Height and surface profile of 3 inlet t-junction of conjugated polymer microfluidic device using laser microscope

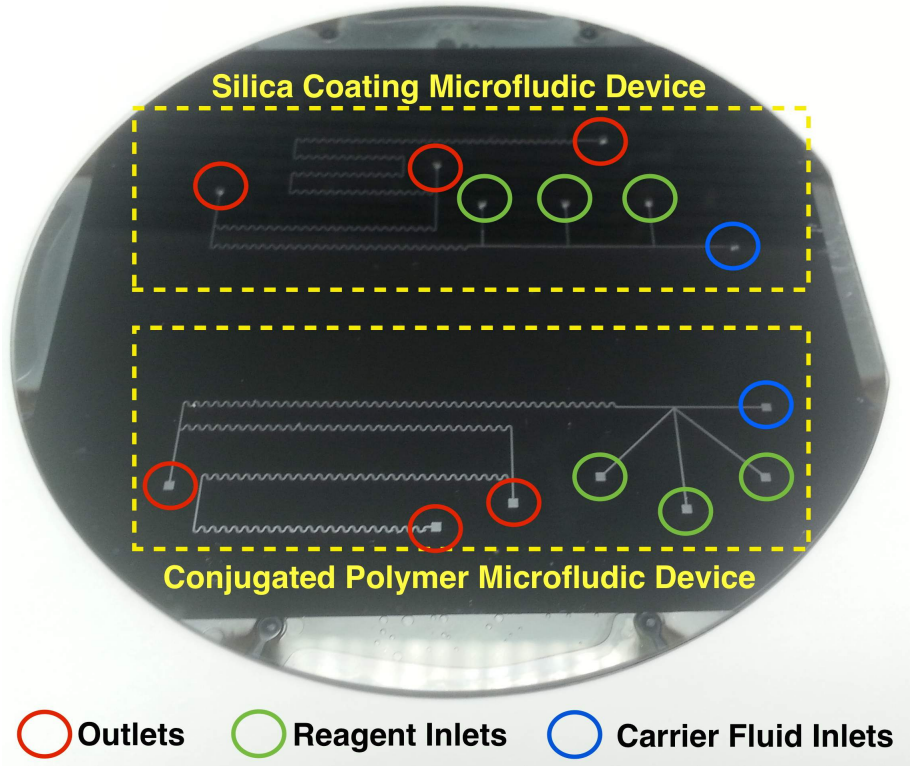

Figure 3.11: Microfluidic device manufactured using photolithography technique on 4" wafer

3.2 Experimental Results

As it is stated in the previous section, machining techniques caused fillet effect problems at the t-junction. Microscope images of different sections of microreactor shall be seen in Figure 3.12.

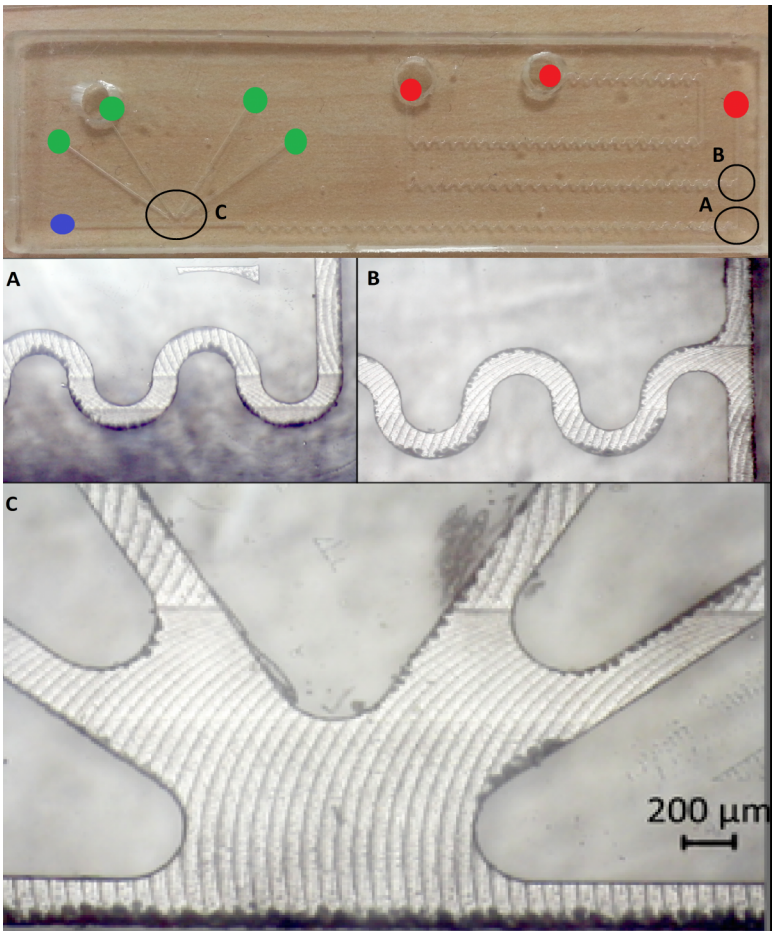

Figure 3.12: Image of manufactured PDMS based microreactor. Green marks denote the inlets for chemicals used in the synthesis, blue mark denotes the inlet for the carrier fluid and red marks show the outlets.

In this section, we have discussed experimental results of silica coating of quantum dots. As preliminary experiments, we have implemented chemicals without quantum dots. According to the theory, with supplied chemicals without quantum dots will form spherical silica nanoparticles [89].

From Figure 3.12, it can be seen that milling could not provide required dimensions from the CAD drawing due to the existence of tool diameter. This issue affected capability of droplet formation of the device highly since droplet formation shear stress is reduced as the area affecting the carrier fluid increased. Additionally, from the same figure, marks of the tool shall be seen which affects surface roughness dramatically. Due to that reason, we came with an alternative solution to this problem. We have used two outlets at the exit as inlet ports, connected with syringe pumps. As a results, we have used junction point at area B instead of C. Experimental setup and silica synthesis flowchart are given in Figure 3.13 and Figure 3.14

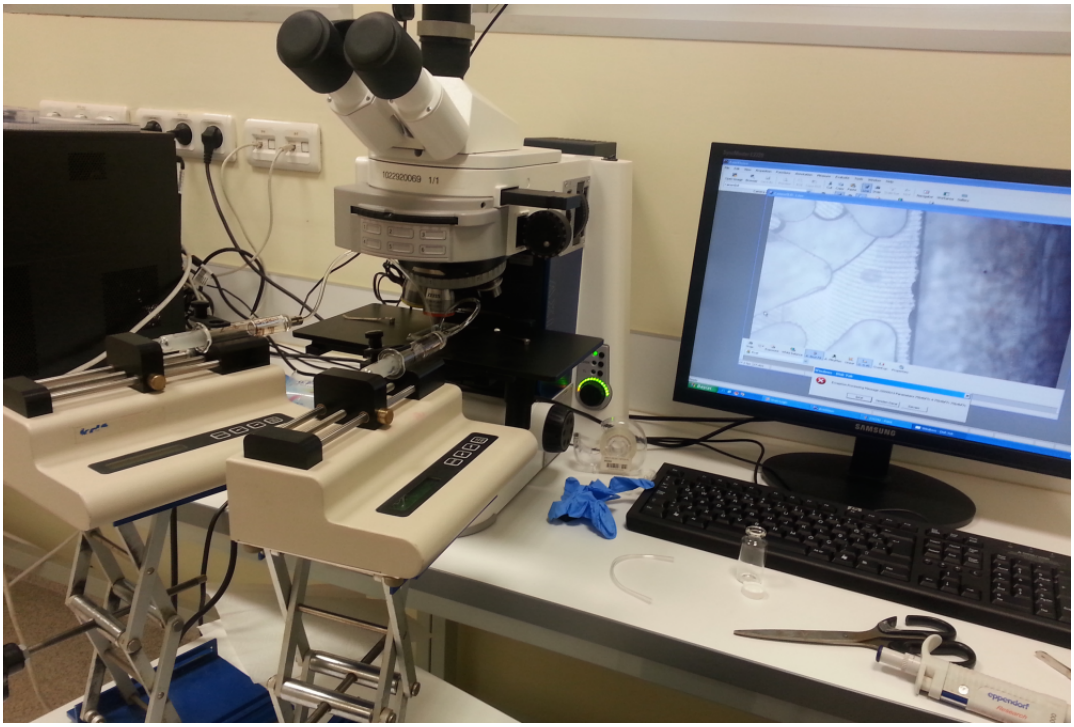

Figure 3.13: Experimental setup of Silica synthesis

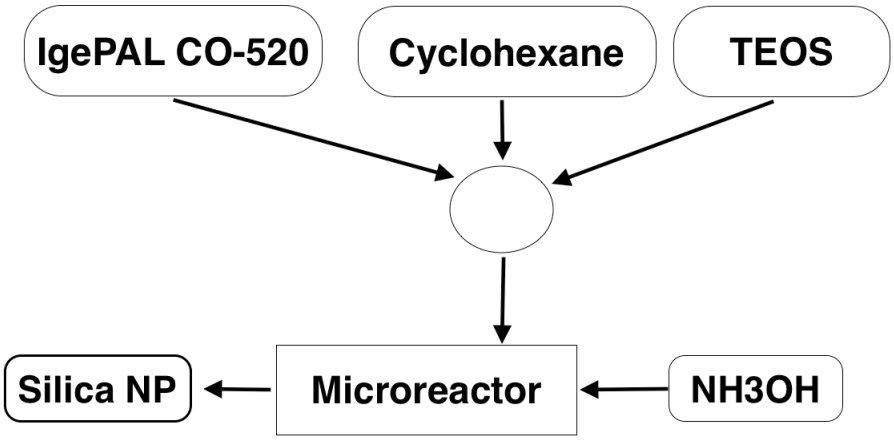

Figure 3.14: Flowchart of Silica synthesis

3.2.1 Silica Synthesis Results

As a preliminary study, we tested the silica formation inside droplets, without including quantum dots during the synthesis and we obtained silica nanoparticles with 102 nm $\pm$ 4 nm diameter. In fact, there are different silica coating methods [90, 91], in the synthesis we followed a modified method of Pietra et. al. where droplets of solution composed of 20 mL Cyclohexane, 2.6 mL IGEPAL and 300 μL TEOS were formed inside the carrier fluid NH_4OH at a flow rate ratio of 2:1 [89]. The total residence time in the reactor was 10 minutes. Afterwards, products from the chemical reaction were mixed with ethanol with 1:1 ratio and samples were centrifuged at 14500 rpm for 10 minutes. Precipitated silica particles were drained from liquid mixture and silica coated quantum dot particles were mixed with distilled water. In order to solve particles inside distilled water, suspensions in the tube were left in the ultrasonic cleaner for 1 hour. After this procedure, particles were imaged under dynamic light scattering (DLS) to obtain data for evaluating the size distribution of particles. It is observed that nanoparticles were synthesized as a result of diffusion and mixing of NH_4OH inside droplets. Size distribution and number of particles and TEM image are given in Figure 3.15 and Figure 3.16.

As it is seen from Figure 3.15, nanoparticles with narrow size of distribution was

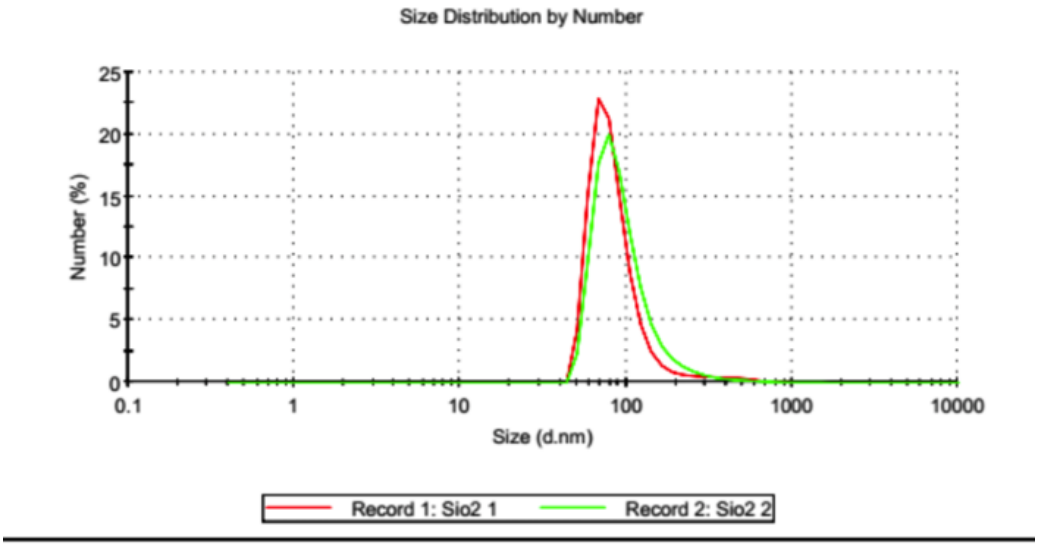

Figure 3.15: Size distribution of particles of microreactor results.

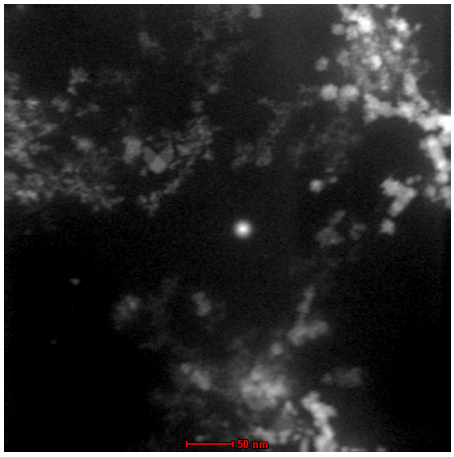

Figure 3.16: TEM image of particles of microreactor results.

successfully synthesized. In fact, from Figure 3.16, it was seen that nanoparticles have agglomerated so that nanoparticles in DLS had large size distribution. The reason of the agglomeration was due to the injection of too much amonium hydroxide as carrier fluid. Since provided amonium hydroxide amount in the microchannels is very high due to 2:1 flow rate ratio compared to given prescription, agglomeration happened between nanoparticles. Additionally, reaction to take 2 mL sample took around 10 minutes. In batch-wise method, this reaction time was 3 days, which can be considered as a great improvement in the manner of reaction time. The matter of fact, amonium hydroxide damaged PDMS

microchannels. Due to that reason, the experiment could only be conducted for 10 minutes. To solve this issue, a silicon based microfluidic device was fabricated using photolithography technique.

3.3 Conclusion

In this section, designed microreactors, according to presented simulation results in Chapter 2 was fabricated. For silica synthesis and coating of quantum dots, microfluidic device mold was fabricated using mechanical microfabrication technique. Due to tool effects on formation zones, we could not form droplets in desired section of microfluidic device. Alternatively, droplets were formed at the junction of one outlet and continuing channel. According to experimental results, silica nanoparticles with 102 nm $\pm$ 4nm were synthesized. Collection 2 mL of sample was collected in 10 minutes using microreactor shall be considered as more practical and fast reaction compared to batch-wise synthesis method in 3 days. Nevertheless, agglomeration between nanoparticles were explained as supplying more than required amonium hydroxide according to the prescription. Additionally, amonium hydroxide damaged PDMS device. Due to that reason, the experiment was only lasted for 10 minutes. To eliminate those drawbacks, a new microfluidic device was fabricated using micromachining technique; however it has not been used for the synthesis yet.

Chapter 4

Conjugated Polymer Nanoparticle (CPN) Synthesis

4.1 Fabrication of the Microfluidic Device

In order to synthesize multilayer conjugated polymer nanoparticles, a new design was proposed, given in Figure 4.1.

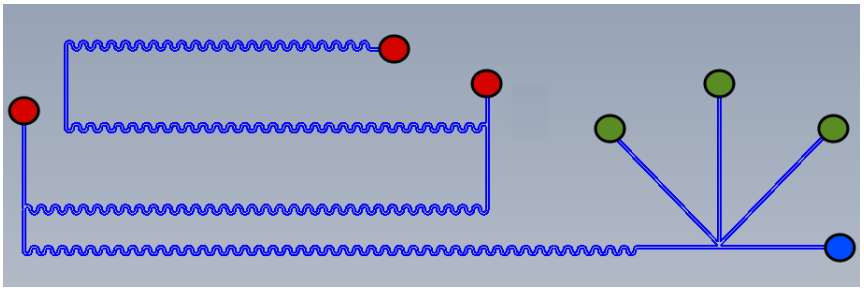

Figure 4.1: CAD Drawing of Conjugated Polymer Synthesis Microreactor. Green marks indicate transporting fluids, blue mark indicates carrier fluid and red marks indicate outlets to analyze residence distribution time.

Flow chart of photolithography fabrication process of conjugated polymer nanoparticle synthesis microreactor is given in Figure 4.2. Spinning speeds and baking times were calculated according to the process guide provided by the

MicroChem company [92].

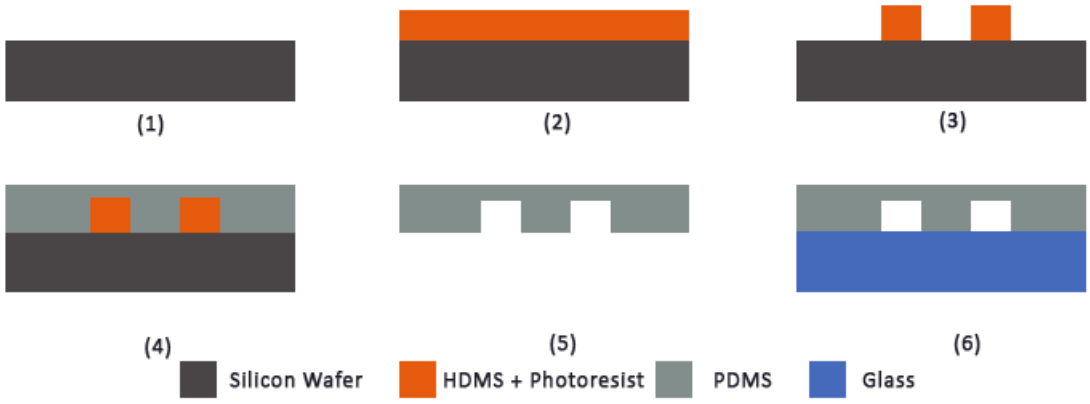

Figure 4.2: Fabrication steps of conjugated polymer nanoparticle synthesis microreactor using photolithography technique

1. Initially, Si wafer was rinsed with Acetone, Isopropanol and deionized (DI) water respectively. Then, wafer was dried with Blow Dry until no water droplet left on both sides of the surface.

2. Wafer was placed in the oven for 7 minutes at 110°C to remove the remaining water particles and moisture on the surface.

3. Cleaned wafer was held in the ambient for 4 minutes to cool down.

4. Cleaned substrate was coated with HDMS and SU-8:2050 (negative photoresist). Spinning time, velocity and acceleration for both chemicals are given respectively: v_{HDMS} = 5000 rpm, a_{HDMS} = 2000rpm/s, t_{HDMS} = 40s; $v_{PR,spread}$ = 500 rpm, $a_{PR,spread}$ = 100 rpm/s, $t_{PR,spread}$ = 10s, $v_{PR,spind}$ = 1000 rpm, $a_{PR,spin}$ = 300 rpm/s, $t_{PR,spin}$ = 30s. Resultant HDMS and PR thickness was 200 μm. The purpose of coating substrate with HDMS was to provide better stiction of photoresist to the substrate. To have a uniform photoresist layer, photoresist should be dropped at a single step, without pouring on the top of already poured photoresist. Having two step spreading of photoresist is due to high viscosity of SU-8:2050 photoresist. Initially, photoresist was spreaded, then spinned at higher rotational speed.

5. Edge beads were removed using acetone and towel.

6. After spinning process, wafer was baked on hot plate at 65°C for 7 minutes and at 95°C for 33 minutes (Soft-bake). To eliminate thermal stress on photoresist and prevent cracks on the surface, substrate was heated at two different temperatures for different times.

7. Baked wafer was held at ambient for 4 hours to let photoresist become harder. Otherwise, substrate would stick to the mask during exposure step.

8. Wafer was exposed to UV light under 275 mJ/cm^2 power with proximity. Separation distance was selected as 200μm, proximity was 500μm, mask thickness was 2.3μm, substrate thickness for a 4 inch wafer was 500μm and resist thickness was 200 μm.

9. Exposed wafer was held on the hot plate at 65°C for 5 minutes and at 95°C for 13 minutes (Post-bake). Post bake time should not be exceeded in order not to have a strong bonding between substrate and photoresist. After the first 15 seconds channels on the substrate was visible. (Otherwise, that means exposure was not done properly.)

10. Baked wafer was held at room temperature for 4 minutes to cool down (Ramp down). If this cool down process was not done, there would have been cracks in the microscopic level on the photoresist.

11. After the cool down process, photoresist was developed in SU-8:2000 developer for 16 minutes. Oppositely from silica synthesis microreactor, developer was not diluted with water. To remove exposed sections of photoresist, substrate with developer was shook all the time, which increased the development speed significantly.

12. Wafer was rinsed with isopropanol and water, later blow dried with N_2. At this step, acetone was not used.

13. Microscopic inspection was done to see if there were any cracks on the photoresist and uniformity of the mold.

14. Finally the substrate with developed photoresist was used for soft lithography technique stated in Appendix B.

Microscope images of polymer synthesis microreactor shall be seen in Figure 4.3 and 4.4.

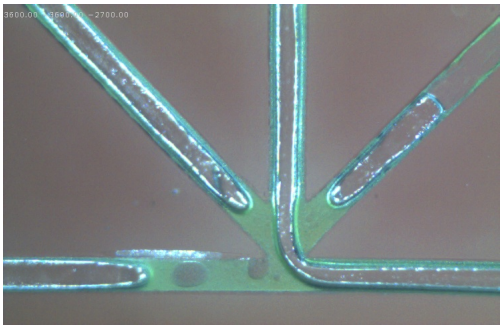

Figure 4.3: Microscope image of star shaped t-junction section of conjugated polymer microreactor

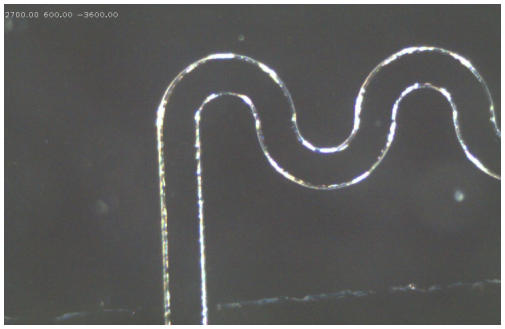

Figure 4.4: Microscope image of sinusoidal section of conjugated polymer microreactor

From microscope images, it is visible that channel quality is good and there is not any fillet effects at the junctions. In the next section experiments held in this fabricated device is discussed.

4.2 Experimental Results

Using the fabricated microfluidic device, synthesis of green emitting conjugated polymer nanoparticle was demonstrated. The experimental set-up and the reactor under the UV light after experiments are shown in Figures 4.5 and 4.6.

4.2.1 Bulk Solution

One of the main goal in this synthesis is to eliminate agglomeration between nanoparticles. Since THF solution and water reacts very fast, agglomeration starts as soon as chemicals were mixed. In this section, we compared results

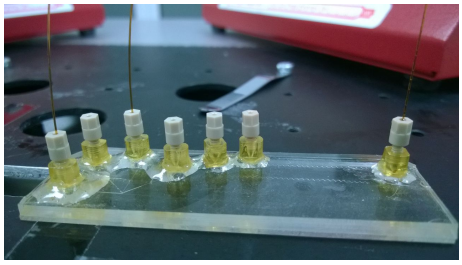

Figure 4.5: Conjugated polymer synthesis microreactor with attached ports.

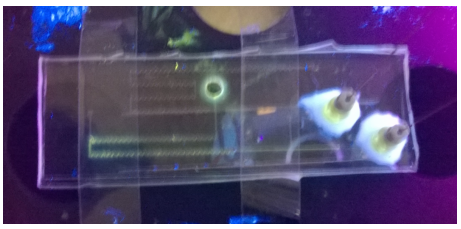

Figure 4.6: Conjugated polymer synthesis microreactor after experimentation under UV light

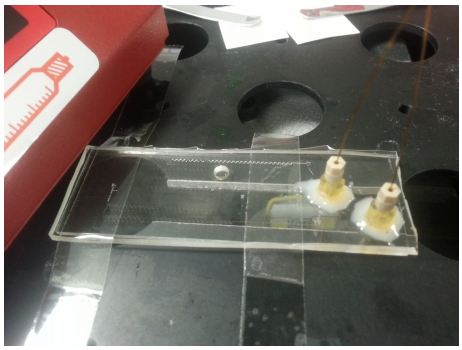

Figure 4.7: Conjugated polymer microreactor before experimentation.

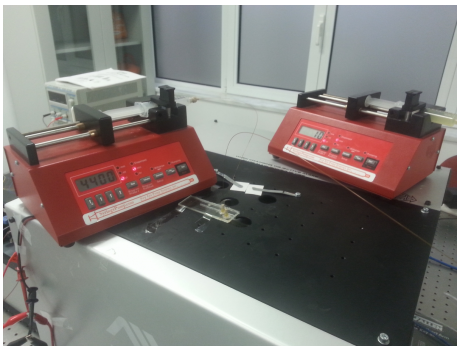

Figure 4.8: Experimental setup of conjugated polymer synthesis

obtained in droplet-based flow and in continuous flow. Before conducting experiments on microreactor, we have analyzed bulk solution using DLS and SEM results. THF and water was mixing at 1:5 ratio inside a test tube. DLS, SEM results of this bulk solution were given in Figure 4.9 and Figure 4.10 and image of bulk sample under UV light was given in Figure 4.11.

As it is seen in Figure 4.9, bulk solution has a nanoparticle size of 1574 nm. As it was explained previously, that size of nanoparticles is due to the agglomeration and this is not desired due to cause of low quality in nanoparticles. In fact, we are aiming to have nanoparticle size around 100 nm with better monodispersity and uniformity. From Figure 4.10, agglomeration between nanoparticles shall be clearly seen. Moreover, distribution distance between nanoparticles are too wide that it is not monodisperse. Therefore, this output would not be used for any commercial application. In order to decrease agglomeration, continuous flow and droplet-based flow was tested by circulating bulk solution.

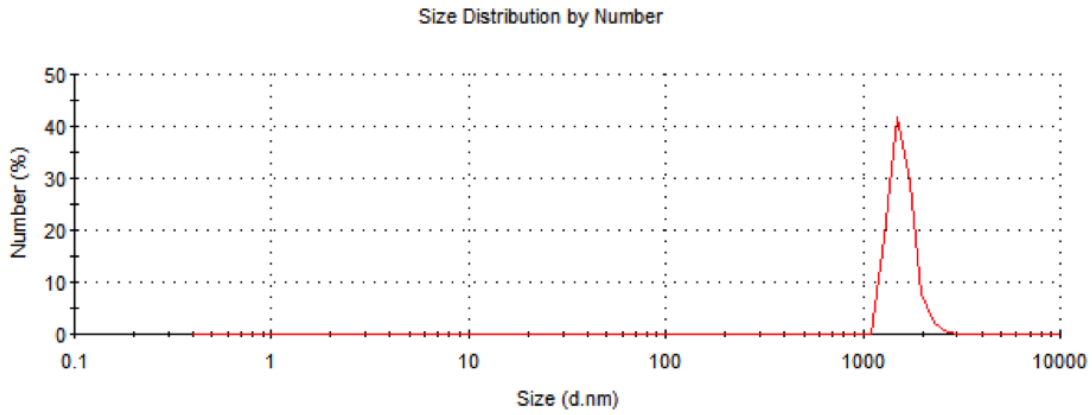

Figure 4.9: DLS result of bulk solution conjugated polymer nanoparticles. Nanoparticle size: 1574 nm ± 15 nm.

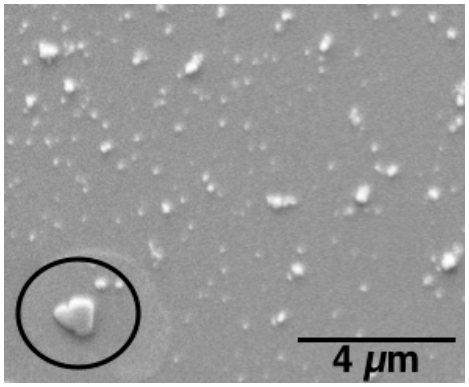

Figure 4.10: SEM result of bulk solution. Agglomeration was indicated in circle.

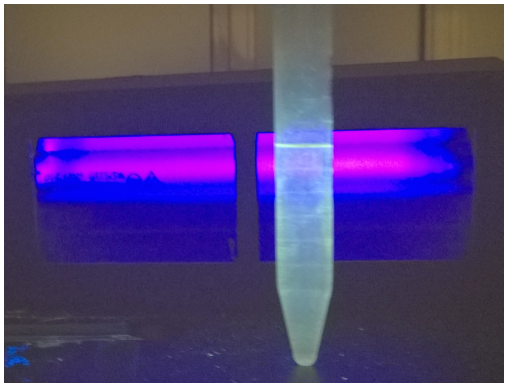

Figure 4.11: Bulk sample under UV light.

4.2.2 Continuous Flow

In this study, we have tested the effect of continuous flow on nanoparticles. As given in Figure 4.1, we have used only single transporting fluid inlet to circulate bulk solution with the flow rate of 55 μL/min. For the carrier fluid, olive oil was used to form the droplets with the flow rate of 30 μL/min. To extract solution, second outlet was used only. As a result, we had a continuous flow starting from the star shaped t-junction. DLS and SEM results of continuous flow output were given in Figure 4.12 and Figure 4.13 and continuous flow inside microchannels were given in Figure 4.14.

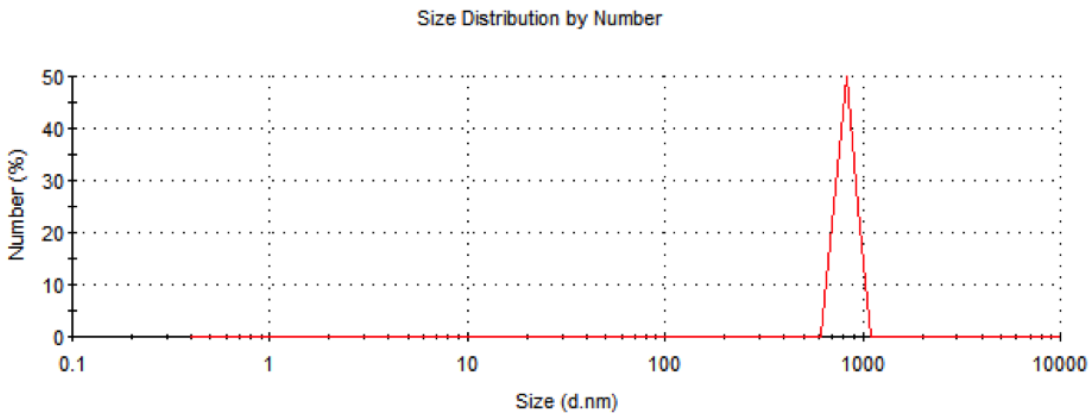

Figure 4.12: DLS result of continuous flow output of conjugated polymer nanoparticles. Nanoparticle size: 826 nm ± 17 nm.

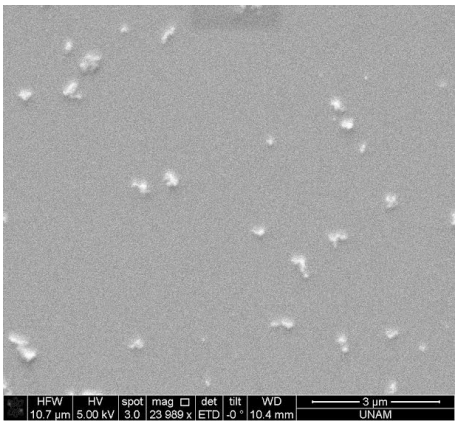

Figure 4.13: SEM result of continuous flow output.

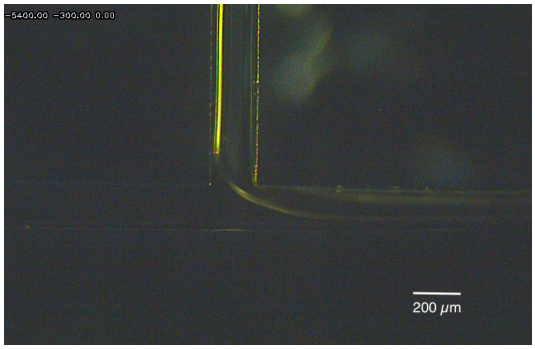

Figure 4.14: Flow inside microchannels using continuous flow.

From Figure 4.14, it can be seen that the continuous flow was successfully implemented. In Figure 4.12, nanoparticles were synthesized with the size of 826 nm. This result is better compared to bulk solution but still not close to the desired value. Additionally, Figure 4.13 shows that nanoparticle distribution is still wide and not monodisperse. Therefore, this method is not useful for desired output quality.

4.2.3 Droplet-Based Flow

In the next step, we have tested droplet-based from using the same inlets for carrier and transporting fluids. Additionally this time, 3 outlets was used in order to analyze residence time. In this case, transporting fluid flow rate was 55 μm/min and carrier fluid flow rate was 15 μm/min. For each outlet, collecting 0.5 ml of sample took approximately 40 minutes. Accordingly, DLS results for each outlet were given in Figure 4.15, Figure 4.16 and Figure 4.17.

From DLS results, we can see that as residence time increases - more circulation - size of nanoparticles reach closer values to desired value. Additionally, more circulation provided more uniformity, percentage of nanoparticles increased and peak in DLS curve becomes sharper. As a result, final nanoparticle size decreased up to 220 nm, which is due to mixing reagent at the outside of the microreactor. Monodispersity of nanoparticles was checked using SEM images, which are given in Figure 4.18 and Figure 4.19. Since we know that nanoparticles from outlet 2 and outlet 3 are closer to the desired value, results from only these outlets were analyzed. From SEM results of droplet-based flow, we can see that even a short synthesis increased monodispersity significantly. Stillnanoparticles are not as monodisperse as desired, but clearly the quality of nanoparticles was better compared to the results obtained from continuous flow. Droplet formation inside microchannels is shown in Figure 4.20 and circulation of droplets at different sections of the sinusoidal part of the microreactor is shown in Figure 4.21.

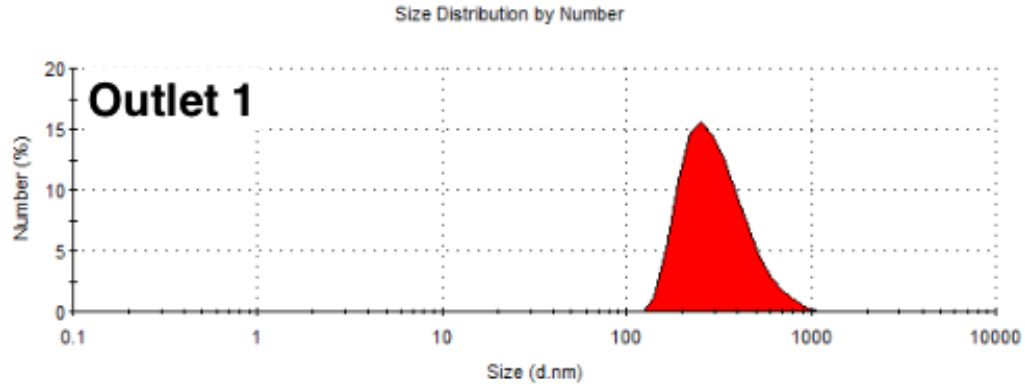

Figure 4.15: DLS result of droplet-based flow products of conjugated polymer nanoparticles from outlet 1. Nanoparticle size: 317 nm ± 15 nm

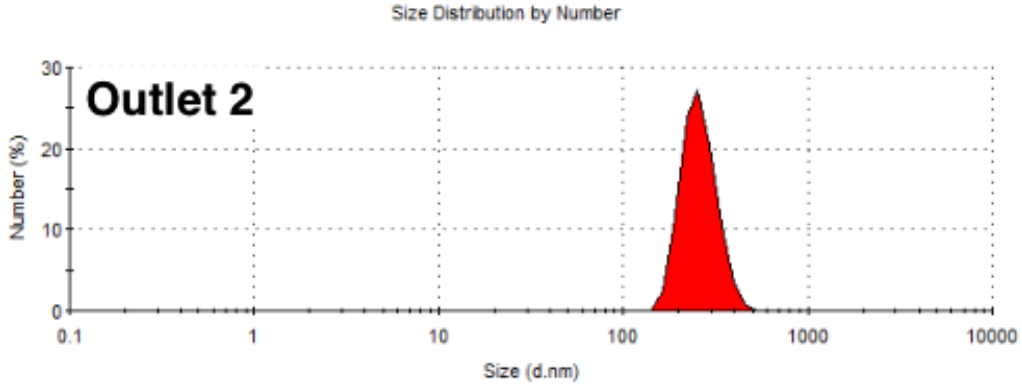

Figure 4.16: DLS result of droplet-based flow products of conjugated polymer nanoparticles from outlet 2. Nanoparticle size: 260 nm ± 12 nm

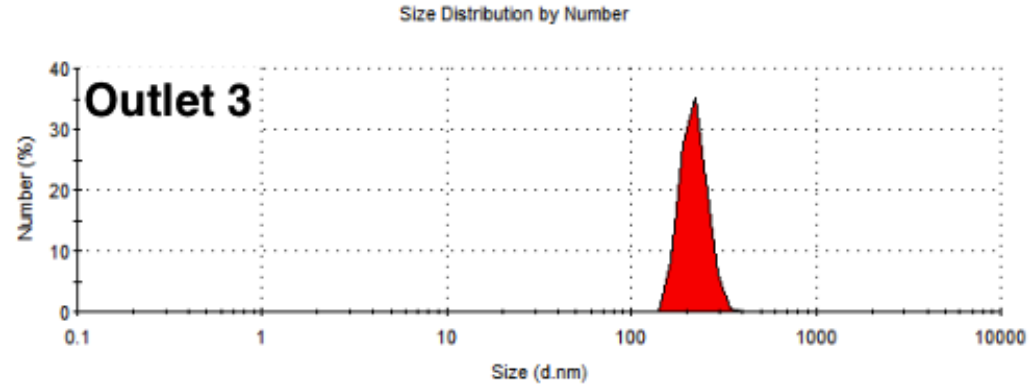

Figure 4.17: DLS result of droplet-based flow products of conjugated polymer nanoparticles from outlet 3. Nanoparticle size: 220 nm ± 9 nm

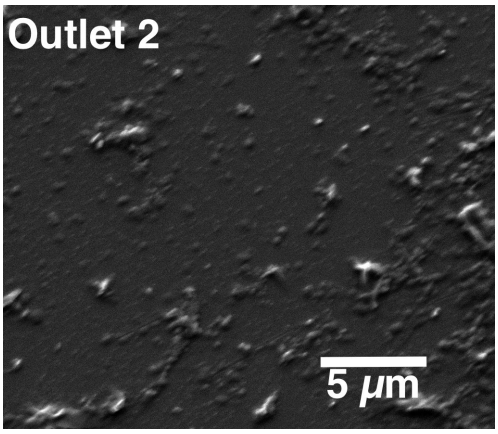

Figure 4.18: SEM image of nanoparticles acquired from outlet 2

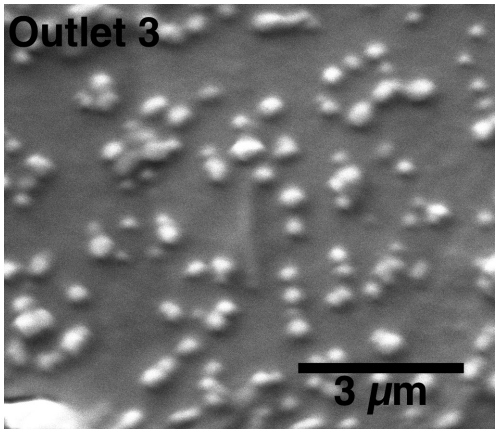

Figure 4.19: SEM image of nanoparticles acquired from outlet

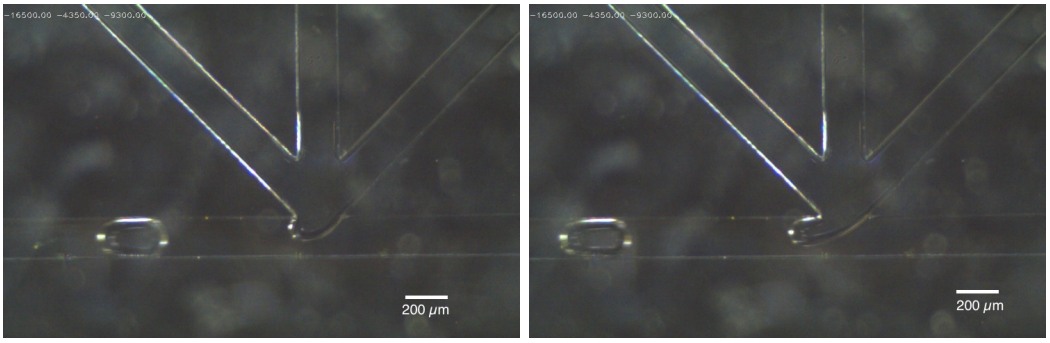

Figure 4.20: Formation of droplets inside microchannels using star shaped t-junction

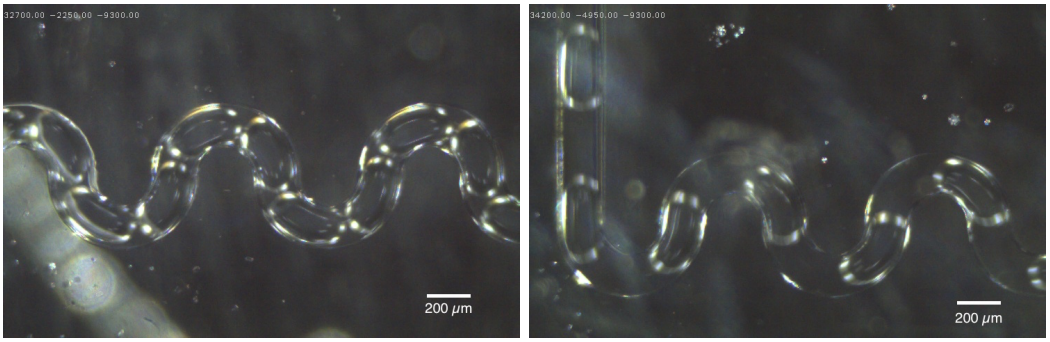

Figure 4.21: Circulation of droplets inside sinusoidal microchannels

4.3 Conclusion

To sum up, the mold of the microreactor for the synthesis of conjugated polymer nanoparticle was fabricated by using microfabrication and microfluidic device was fabricated using soft lithography method out of this mold. Synthesis of green CPN was performed using three different methods: batch-wise, continuous flow and droplet-based flow. In batch-wise synthesis results it has been seen that nanoparticle size was extremely high and dispersed. Additionally, high level of agglomeration was observed. Using continuous flow in the microreactor, agglomeration was reduced. However, the level of monodispersity and uniformity was still not good enough for commercial applications. As a final study, droplet-based flow was used to synthesize CPNs. From the results it has been seen that, this method provided much better uniformity and mondispersity compared to the previous methods. Comparison of all these methods with respect to the nanoparticle sizes is given in Figure 4.22.

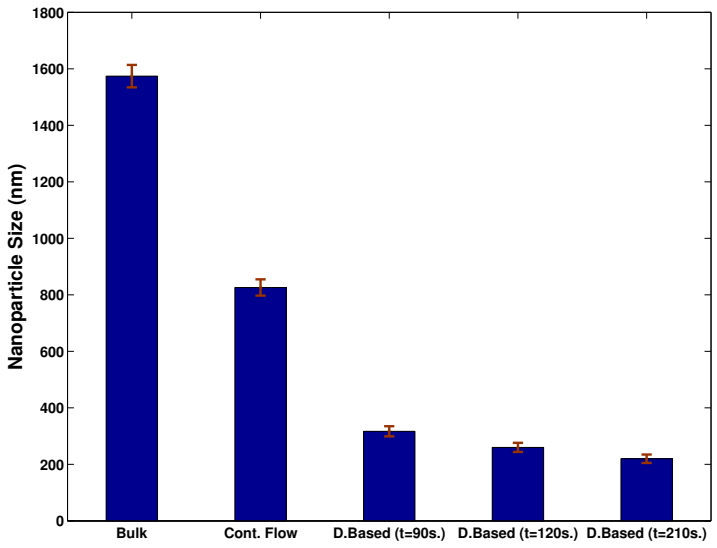

Figure 4.22: Overall results of nanoparticle sizes with different synthesis methods

From the results, we can see that, droplet-based flow significantly improved nanoparticle sizes at the output. Not only better compared to other methods but more circulation inside microchannels improved nanoparticle size as well.

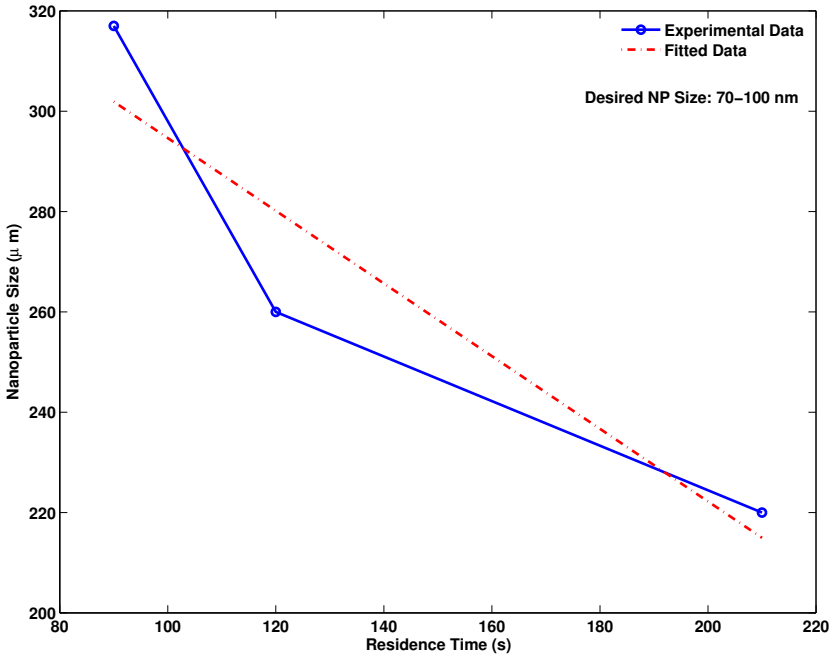

Figure 4.23: Nanoparticle size with respect to residence time of CPNs

Chapter 5

Conclusion and Suggested Future Works

To sum up, in this thesis multiple microreactors have been proposed for silica coating of quantum dots and synthesis of conjugated polymer nanoparticles. At the design section of this study, a set of Comsol Multiphysics simulations have been conducted to test mixing performance in microchannels by tracking the location of spherical nanoparticles inside droplets for various geometries. By looking at the results of simulations, we have concluded that smaller microchannels show better performance in the manner of velocity peaks, vertical particle displacements and dispersion length difference between released particles. As a future work, testing mixing performances at different flow rate ratios would be a good contribution to the literature.

Microreactors were designed based on the simulation results. Microreactors was manufactured as small as possible. For silica coating microreactor mold, firstly micromachining technique have been used. Later on, using soft-lithography technique, manufacturing of the microreactor was completed. Due to the effect of milling tool on the junctions, droplet formation became a problematic issue. A set of preliminary experiments was conducted using this microreactor using an alternative scheme. Later on, the design have been changed and microreactor

was manufactured using photolithography technique and Bosch process. For conjugated polymer synthesis microreactor, photolithography technique was used. Again, to form microchannels we have used soft-lithography technique.

Using manufactured microreactors, silica coating performance was tested without implementing quantum dot nanoparticles. According to the formation of spherical silica nanoparticles, we have acquired silica nanoparticle size with 102 nm $\pm$ 4 nm in 10 minutes. This reaction time can be considered as a good result since for batch-wise experiments, synthesis time is around 3 days. For conjugated polymer nanoparticle synthesis, we have compared bulk solution, continuous flow and droplet-based flow. As a result, droplet-based flow prevented most of the agglomeration happened in bulk solution and shown better performance compared to continuous flow.

As conjugated polymer microreactor was manufactured, bulk solution, continuous flow and droplet-based flow was tested as preliminary experiments. As a result, bulk solution came up with high level of agglomeration, low monodispersity and non-uniform nanoparticle distribution. In fact, continuous flow provided better distribution of size and uniformity. Matter of fact, droplet-based flow provided closer nanoparticle size to the desired value and better monodispersity and uniformity compared to other methods. In addition to that, circulation of droplets more in microchannels increased monodispersity and uniformity of nanparticles.

Bibliography

[1] R. P. Feynman, *There's Plenty of Room at the Bottom*, Engineering and Science, vol. 23 (5), pp. 22-36, 1960.

[2] T. Zhanga, X. Zhanga, X. Yana, L. Konga, G. Zhanga, H. Liua, J. Qiua, K. L. Yeungb K., *Synthesis of Fe_3O_3 ZIF_8 magnetic coreshell microspheres and their potential application in a capillary microreactor*, Chemical Engineering Journal, vol. 228, pp. 398-404, 2013.

[3] G. M. Greenwaya, S. J. Haswella , D. O. Morganb, V. Skeltona, P. Styringa, *The use of a novel microreactor for high throughput continuous flow organic synthesis*, Sensors and Actuators B: Chemical, vol. 63, pp. 153-158, 2000.

[4] J. Wanga, S. S. Gub, H. S. Cuib, L. Q. Yanga, X. Y. Wua, *Rapid synthesis of propyl caffeate in ionic liquid using a packed bed enzyme microreactor under continuous-flow conditions*, Bioresource Technology, vol. 149, pp 367-374, 2013.

[5] P. M. Valencia, O. C. Farokhzad, R. Karnik, R. Langer, *Microfluidic technologies for accelerating the clinical translation of nanoparticles*, Nature Nanotechnology, vol. 7, pp. 623-629, 2012.

[6] E. K. Sackmann, A. L. Fulton, D. J. Beebe, *The present and future role of microfluidics in biomedical research*, Nature, vol. 507, pp. 181-189, 2014.

[7] C. A. Baker, C. T. Duong, A. Grimley, M. G. Roper, *Recent advances in microfluidic detection systems*, Bioanalysis, vol. 1(5), pp. 967-975, 2009.

[8] A. M. Streets, Y. Huang, *Chip in a lab: Microfluidics for next generation life science research*, Biomicrofluidics, vol. 7, 011302, 2013.

[9] S. Sukhatme, A. Agarwal, *Digital Microfluidics: Techniques, Their Applications and Advantages*, J Bioengineer & Biomedical Sci, S8:001, 2012.

[10] C. X. Zhaoa, L. Hea, S. Z. Qiaob, A. P.J. Middelberg, Nanoparticle synthesis in microreactors, Chemical Engineering Science, vol. 66(7), pp. 1463-1479, 2011.

[11] L. Frenz, A. E. Marrak, M. Pauly, S. Begin-Colin, A. D. Griffiths, *Droplet-Based Microreactors for the Synthesis of Magnetic Iron Oxide Nanoparticles*, Angew. Chem. Int. Ed., vol. 47, pp. 6817-6820, 2008.

[12] H. Hung, A. P. Lee,*Microfluidic Devices for the Synthesis of Nanoparticles and Biomaterials*, Journal of Medical and Biological Engineering, vol. 27, pp. 1-6, 2007.

[13] J. D. Winterton, *Development of a Novel Microfluidic Reactor for Highly Controlled Synthesis of Semiconductor Nanocrystals*, PhD Dissertation, University of California Berkeley, 2008.

[14] L. Gutierreza, L. Gomeza, S. Irustaa, M. Arrueboa, J. Santamariaa, *Comparative study of the synthesis of silica nanoparticles in micromixer-microreactor and batch reactor systems*, Chemical Engineering Journal, vol. 171(2), pp. 674-683, 2011.

[15] X. Ma, W. Y. Tseng, M. Eddings, P. Y. Kenga, R. M. V. Dam, *A microreactor with phase-change microvalves for batch chemical synthesis at high temperatures and pressures*, Lab on a Chip, vol. 14(2), pp. 280-285, 2014.

[16] S. Marre, J. Baek, J. Park, M. G. Bawendi, K. F. Jensen, *High-Pressure/High-Temperature Microreactors for Nanostructure Synthesis*, Journal of Laboratory Automation, vol. 14(6), pp. 367-373, 2009.

[17] T. Rahman, E. V. Rebrov, *Microreactors for Gold Nanoparticles Synthesis: From Faraday to Flow*, Processes, vol. 2, pp. 466-493, 2014

[18] A.D. Stroock, S.K. Dertinger,A. Ajdari, I. Mezic, H. A. Stone, G. M. Whitesides, *Chaotic Mixer for Microchannels* Science, vol. 295(5555), pp. 647-51, 2002.

[19] N. Pamme, *Continuous flow separations in microfluidic devices.* Lab on a Chip, vol. 7, 1644-1659, 2007.

[20] A. Jahn, J. E. Reiner, W. N. Vreeland, D. L. DeVoe, L. E. Locascio, M. Gaitan, *Preparation of nanoparticles by continuous-flow microfluidics.* J Nanopart Res, vol. 10, pp. 925-934, 2008.

[21] D. P. Kise, D. Magana, M. J. Reddisha, R. B. Dyer, *Submillisecond mixing in a continuous-flow, microfluidic mixer utilizing mid-infrared hyperspectral imaging detection.* Lab on a Chip, vol. 14(3), pp. 584-591, 2014.

[22] M. W. Wang, *Combined Microfluidic-Eectric Diffused Mixing of Living Cells in Continuous Flow.* Japanese Journal of Applied Physics, vol. 49, 024205, 2009.

[23] T. M. Tran, F. Lan, C. S. Thompson, A. R. Abate, *From Tubes to Drops: Droplet-Based Microfluidics for Ultrahigh-Throughput Biology*, J. Phys. D: Appl. Phys., vol. 46(11), 114004, 2013.

[24] B. Cetin, M. D. Asik, S. Taze, *Design and Fabrication of a Microfluidic Device for Synthesis of Chitosan Nanoparticles*, Journal of Nanotechnology in Engineering and Medicine, vol. 4, 031004, 2013.

[25] E. Y. Erdem, J. C. Cheng, F. M. Doyle, A. P. Pisano, *Multi-Temperature Zone, Droplet-based Microreactor for Increased Temperature Control in Nanoparticle Synthesis,* Small, vol. 10(6), pp. 1076-1080, 2014.

[26] E. Y. Erdem, *Microfluidic Reactors for the Controlled Synthesis of Nanoparticles*, Ph.D. Dissertation, University of California Berkeley, 2013.

[27] L. Frenz, A. E.Harrak, M. Pauly, S. B. Colin, A. Griffiths, J. C. Baret, *Droplet-Based Microreactors for the Synthesis of Magnetic Iron Oxide Nanoparticles*, Angewandte Chemie International Edition, vol. 47(36), pp. 6817-6820, 2008.

[28] I. Shestopalov, J. D. Ticea, R. F. Ismagilov, *Multi-step synthesis of nanoparticles performed on millisecond time scale in a microfluidic droplet-based system*, Lab on a Chip, vol. 4, pp. 316-321, 2004.

[29] I. L. Medintz, H. Mattoussi, A. R. Clapp, *Potential clinical applications of quantum dots*, International Journal of Nanomedicine, vol. 8(2), pp. 151167, 2008.

[30] D. Bera, L. Qian, T. K. Tseng, P. H. Holloway, *Quantum Dots and Their Multimodal Applications: A Review*. Materials, vol. 3, pp. 2260-2345, 2010.

[31] R. Plass, S. Pelet, J. Krueger, M. Gratzel, U. Bach, *Quantum dot sensitization of organic-inorganic hybrid solar cells*. J. Phys. Chem. B, vol. 106, pp. 7578-7580, 2002.

[32] S. Mahajan, M. Rani, R. B. Dubey, J. Mahajan, *Characteristics and properties of CdSe Quantum Dots*. International Journal of Latest Research in Science and Technology, vol. 2(1), pp 457-459, 2002.

[33] K. K. Likharev, *Single-electron devices and their applications*, Proceedings of the IEEE, vol. 87, pp. 606632, 1999.

[34] F. H. L. Koppens, C. Buizert, K. J. Tielrooij, I. T. Vink, K. C. Nowack, T. Meunier, L. P. Kouwenhoven, L. M. K. Vandersypen, *Driven coherent oscillations of a single electron spin in a quantum dot*, Nature, vol. 442, pp. 766771, 2006.

[35] D. Loss, D. P. DiVincenzo, *Quantum computation with quantum dots*, Physical Review A, vol. 57(1), pp. 120-126, 1998.

[36] L. Qian, D. Bera, T K. Tseng, P. H. Holloway, *High efficiency photoluminescence from silica-coated CdSe quantum dots.* Applied Physics Letters, vol. 94(7), 073112, 2009.

[37] M. Vibin, R. Vinayakan, A. John, F. B. Fernandez, A. Abraham, *Effective cellular internalization of silica-coated CdSe quantum dots for high contrast cancer imaging and labelling applications.* Cancer Nanotechnology vol. 5(1), 2014.

[38] C. Maoquan, S. Ye, X. Sh, *Silica-coated quantum dots fluorescent spheres synthesized using a quaternary 'water-in-oil' microemulsion system.* Journal of Nanoparticle Research, vol. 10(4), pp. 613-624, 2008.

[39] X. Li, F. J. Kao, C. C. Chuang, S. He, *Enhancing fluorescence of quantum dots by silica-coated gold nanorods under one-and twophoton excitation.* Optics Express, vol. 18(11), 11335, 2010.

[40] A. Wolcott, D. Gerion, M. Visconte, J. Sun, A. Schwartzberg, S. Chen, J. Z. Zhang, *Silica-Coated CdTe Quantum Dots Functionalized with Thiols for Bioconjugation to IgG Proteins.* J. Phys. Chem. B, vol. 110, pp. 5779-5789, 2006.

[41] M. J. Park, J. Lee, I. H. Jung, J. H. Park, D. H. Hwang and Hong-Ku Shim, *Synthesis, Characterization and Electroluminescence of Polyuorene Copolymers with Phenothiazine Derivative; Their Applications to High-Efciency Red and White PLEDs.* Macromolecules, vol. 41, pp. 9643-9649, 2008.

[42] Z. Zhang, P. Yan, S. Yue, Y Chen, Q. Wu, D. Qu, R. Guo, P. Wang, Y. Zhao , S. Liu, *Low driving voltage white organic light-emitting diodes with high efficiency and low efficiency roll-off.* Organic Electronics, vol. 14, pp. 21722176, 2013.

[43] Y. Sun, N. C. Giebink, H. Kanno, B. Ma, M. E. Thompson, S.R. Forrest, *Management of singlet and triplet excitons foreefficient white organic light-emitting devices.* Nature, vol. 440, pp. 908-912, 2006.

[44] G. Schwartz, M. Pfeiffer, S. Reineke, K. Walzer, K. Leo, *Harvesting Triplet Excitons from Fluorescent Blue Emitters in White Organic Light-Emitting Diodes.* Adv. Mater., vol. 19, pp. 36723676, 2007.

[45] V. Ibrahimova, M.E. Kocak, A. M. Onal, D. Tuncel, *Optical and Electronic Properties of Fluorene-Based Copolymers and Their Sensory Applications.* Journal of Polymer Science, Part A: Polymer Chemistry, vol. 51, pp. 815823, 2013.

[46] T. Ahn, H. K. Shim, *Synthesis and Luminescent Properties of Blue Light Emitting Polymers Containing both Hole and Electron Transporting Units.* Macromol. Chem. Phys., vol. 202, pp. 3180, 2001.

[47] R. Karnik, F. Gu, P. Basto, C. Cannizzaro, L. Dean, W. Kyei-Manu, R. Langer, O. C. Farokhzad, *Microfluidic platform for controlled synthesis of polymeric nanoparticles*, Nano Letters, vol. 8(9), pp. 2906-2912, 2008.

[48] H. Dogana, S. Nasb, M. Muradoglu, *Mixing of miscible liquids in gas-segmented serpentine channels.* International Journal of Multiphase Flow, vol. 35(12), pp. 1149-1158, 2009.

[49] D. M. Fries, S. Waelchli, P. R. von Rohr, *Gas-liquid two-phase flow in meandering microchannels.* Chemical Engineering Journal, vol. 135(1), pp. S37-S45, 2008.

[50] C. Y. Wu, R. T. Tsai, *Fluid mixing via multidirectional vortices in converging-diverging meandering microchannels with semi-elliptical side walls.* Chemical Engineering Journal, vol. 217, pp. 320-328, 2013.

[51] H. Song, M. R. Bringer, J. D. Tice, C. J. Gerdts, and R. F. Ismagilov, *Experimental test of scaling of mixing by chaotic advection in droplets moving through microfluidic channels,* Appl Phys Lett., vol. 83(12), pp. 4664-4666, 2003.

[52] H. Song, J. D. Tice, and R. F. Ismagilov, *A Microfluidic System for Controlling Reaction Networks in Time,* Angew. Chem. Int. Ed., vol. 42(7), pp. 768-772, 2003.

[53] A. M. Huebner, C. Abell, W. T. S. Huck, C. N. Baroud, F. Hollfelder, *Monitoring a Reaction at Submillisecond Resolution in Picoliter Volumes,* Anal. Chem., vol. 83, pp. 1462-1468, 2011.

[54] E. Y. Erdem, J. C. Cheng, F. M. Doyle, A. P. Pisano, *Multi-Temperature Zone, Droplet-based Microreactor for Increased Temperature Control in Nanoparticle Synthesis,* Small, vol. 10(6), pp. 1076-1080, 2014.

[55] J. D. Tice, H. Song, A. D. Lyon, R. F. Ismagilov, *Formation of Droplets and Mixing in Multiphase Microfluidics at Low Values of the Reynolds and the Capillary Numbers,* Langmuir, vol. 19, pp. 9127-9133, 2009.

[56] M. R. Bringer, C. J. Gerdts, H. Song, J. D. Tice, R. F. Ismagilov, *Microfluidic systems for chemical kinetics that rely on chaotic mixing in droplets.* Philos. Trans. R. Soc. London, Ser. A, vol. 362(1818), pp. 1087-104, 2004.

[57] M. Srisa-Art, A. J. deMello, J. B. Edel, *Fluorescence Lifetime Imaging of Mixing Dynamics in Continuous-Flow Microdroplet Reactors,* PRL 101, 014502, 2008.

[58] R. Chabreyrie, D. Vainchtein, C. Chandre, P. Singh, N. Aubry, *Using resonances to control chaotic mixing within a translating and rotating droplet,* Commun Nonlinear Sci Numer Simulat, vol. 15, pp. 2124-2132, 2010.

[59] R. Chabreyrie, D. Vainchtein, C. Chandre, P. Singh, N. Aubry, *Robustness of tuned mixing within a droplet for digital microfluidics,* Mechanics Research Communications, vol. 36, pp. 130-136, 2009.

[60] W. Lee, G. Son, *Numerical study of obstacle configuration for droplet splitting in a microchannel,* Computers & Fluids, vol. 84 pp. 130-136, 2013.

[61] J. Maddala, R. Rengaswamy, *Design of multi-functional microfluidic ladder networks to passively control droplet spacing using genetic algorithms,* Computers and Chemical Engineering, vol. 60 pp. 413-425, 2014.

[62] L. Wu, M. Tsutahara, L. S. Kim, M. Ha, *Three-dimensional lattice Boltzmann simulations of droplet formation in a cross-junction microchannel,* International Journal of Multiphase Flow, vol. 34, pp. 852-864, 2008.

[63] J. Wanga, D. Yua, H. Jinga, J. Tao, *Hydrodynamic control of droplets coalescence in microfluidic devices to fabricate two-dimensional anisotropic particles through boundary element method,* Chemical Engineering Research and Design, vol. 92, pp. 2223-2230, 2014.

[64] C. Chung, K. Hyun Ahn, S. J. Lee, *Numerical study on the dynamics of droplet passing through a cylinder obstruction in confined microchannel flow,* J. Non-Newtonian Fluid Mech., vol. 162, pp. 38 - 44, 2009.

[65] Y. Yan, D. Guo, S.Z. Wen, *Numerical simulation of junction point pressure during droplet formation in a microfluidic T-junction,* Chemical Engineering Science, vol. 84, pp. 591-601, 2012.

[66] S. Bashir, J. M. Rees, W. B. Zimmerman, *Simulations of microfluidic droplet formation using the two-phase level set method,* Chemical Engineering Science, vol. 66, pp. 4733-4741, 2011.

[67] M. Sussman and E. G. Puckett, *A Coupled Level Set and Volume-of-Fluid Method for Computing 3D and Axisymmetric Incompressible Two-Phase Flows,* Journal of Computational Physics, vol. 162, pp. 301-337, 2000.

[68] A. A. Zaidi, T. Tsuji, T. Tanaka, *A new relation of drag force for high Stokes number monodisperse spheres by direct numerical simulation,* Advanced Powder Technology, vol. 25, pp. 1860-1871, 2012.

[69] H. Bruss, *Theoretical Microfluidics,* Oxford University Press, New York, 2008.

[70] W. B. Zimmerman, G. M. Homsy, *Nonlinear viscous fingering in miscible displacement with anisotropic dispersion,* Physics of Fluids A, vol. 3 (8), pp. 1859-1872, 1991.

[71] H. Bruss, *Viscous fingering in miscible displacements: Unification of effects of viscosity contrast, anisotropic dispersion, and velocity dependence of dispersion on nonlinear finger propagation,* Physics of Fluids A, vol. 4 (11), pp. 2348-2359, 1992.

[72] S. van der Graaf, T. Nisisako, C. G. P. H. Schroen, R. G. M. van der Sman, R. M. Boom, *Lattice Boltzmann Simulations of Droplet Formation in a T-Shaped Microchannel,* Langmuir, vol. 22, pp. 4144-4152, 2006.

[73] W. B. Zimmerman, *Multiphysics Modelling with Finite Element Methods,* World Scientific Series on Stability, Vibration and Control of Systems, vol. 18, Singapore, 2006.

[74] K. B. Deshpande, W. B. Zimmerman, *Simulation of interfacial mass transfer by droplet dynamics using the level set method,* Chemical Engineering Science, vol. 61 pp. 6486-6498, 2006.

[75] K. B. Deshpande, W. B. Zimmerman, *Simulations of mass transfer limited reaction in a moving droplet to study transport limited characteristics,* Chemical Engineering Science, vol. 61 pp. 6424-6441, 2006.

[76] S. Naher, D. Orpen, D. Brabazon, C.R. Poulsen, M.M. Morshed, *Effect of micro-channel geometry on fluid flow and mixing,* Simulation Modelling Practice and Theory, vol. 19, pp. 1088-1095, 2011.

[77] L. Jiang, Y. Zeng, H. Zhou, J. Y. Qu, S. Yao, *Visualizing millisecond chaotic mixing dynamics in microdroplets: A direct comparison of experiment and simulation,* Biomicrofluidics 6, 012810, 2012.

[78] J. Yoon, B. Kim, Y. Choi, E. Yoon, *3-D Lithography and Metal Surface Micromachining for RF and Microwave MEMS,* The Fifteenth IEEE International Conference on Micro Electro Mechanical Systems, Las Vegas, NV, USA, pp 673-676, 2002.

[79] K. D. Vora, B. Lochel, E. C. Harvey, J. P. Hayes, A. G. Peele, *AFM-measured surface roughness of SU-8 structures produced by deep x-ray lithography,* Journal of Micromechanics and Microengineering Vol. 16(10), pp 1975-1983, 2006.

[80] A. Yoshida, Y. Kojima, K. Matsuoka, Y. Tomo, I. Shimizu, M. Yamabe, *Study of resist surface roughness in EB lithography,* Microelectronic Engineering, vol. 53 (1-4), pp 313-316, 2000.

[81] W. Chen, R. H. W. Lam, J. Fu, *Photolithographic surface micromachining of polydimethylsiloxane (PDMS),* The Royal Society of Chemistry, vol. 12(2), pp 391-395, 2012.

[82] J. Frienda, L. Yeo *Fabrication of microfluidic devices using polydimethylsiloxane,* The Biomicrofluidics, vol. 4(2), 026502, 2010.

[83] V. D. R. Michael, *Solvent-resistant elastomeric microfluidic devices and applications,* PhD Dissertation, Califonia Insitute of Technology (CalTECH), 2006.

[84] A. Adamatzky, T. Schubert, *Slime mold microfluidic logical gates,* Materials Today, vol. 17(2), pp 86-91, 2014.

[85] Clariant, *AZ 4500 Series Thick Positive Photoresist Data Sheet*, www.microchemicals.com, 2015.

[86] J. Quero, F. Perdigones, C. Aracil, *Microfabrication technologies used for creating smart devices for industrial applications*, Smart Sensors and MEMS, Woodhead Publishing, 2014.

[87] J. X. Zhang, K. Hoshino, *Fundamentals of nano/micro-fabrication and effect of scaling, Molecular Sensors and Nanodevices*, Oxford: William Andrew Publishing, 2014

[88] M. J. Madou, *Fundamentals of microfabrication : the science of miniaturization*, Boca Raton : CRC Press, 2002.

[89] F. Pietra, R. J. A. V. Dijk - Moes, X. Ke, S. Bals, G. V. Tendeloo, C. D. M. Donega, D. Vanmaekelbergh, *Synthesis of Highly Luminescent Silica-Coated CdSe/CdS Nanorod*, Chem. Mater, vol. 25(17), pp. 3427-3434, 2013.

[90] I. Santana, A. Pepe, E. Jimenez-Pique, S. Pellice, I. Milosev, S. Cere, *Corrosion protection of carbon steel by silica-based hybrid coatings containing cerium salts: Effect of silica nanoparticle content*, Surface & Coatings Technology, 2015.

[91] H. Ishii, S. Ito, D. Nagao, M. Konno, *Ceria nanoparticle vesicles formed in sodium oleate aqueous solution with mesoporous silica coating*, Colloids and Surfaces A: Physicochemical and Engineering Aspects, vol. 441, pp. 638- 642, 2014.

[92] MicroChem, *SU-8 2000 Permanent Epoxy Negative Photoresist Processing Guidelines*, www.microchem.com, 2015.

Appendix A

Developed Code for Particle Tracing in Simulations

```
%{
**************************************************************************
BilMECH Summer 2014 - Particle in Droplet Analysis and Config. Code
Author: Alican Ozkan
Date: 22.06.2014
**************************************************************************
%}
clear all; close all; clc;
%[x_disp, y_disp, z_disp, particle, time, v_x, v_y, v_z, col] = ...
%    textread('codeSinus.txt', '%f %f %f %f %f %f %f %f %f',1000);
[x_disp_1, y_disp_1, z_disp_1, particle_1, time_1, v_x_1, v_y_1, v_z_1, ...
 col_1] = textread('sinus1.txt', '%f %f %f %f %f %f %f %f %f',10000);
[x_disp_2, y_disp_2, z_disp_2, particle_2, time_2, v_x_2, v_y_2, v_z_2, ...
col_2] = textread('sinus2.txt', '%f %f %f %f %f %f %f %f %f',10000);
[x_disp_3, y_disp_3, z_disp_3, particle_3, time_3, v_x_3, v_y_3, v_z_3, ...
col_3] = textread('sinus3.txt', '%f %f %f %f %f %f %f %f %f',10000);
[x200_disp_1, y200_disp_1, z200_disp_1, particle200_1, time200_1, v200_x_1,...
    v200_y_1, v200_z_1, col200_1] = ...
    textread('radius1.txt', '%f %f %f %f %f %f %f %f %f',10000);
```

```
[x200_disp_2, y200_disp_2, z200_disp_2, particle200_2, time200_2, v200_x_2, ...
    v200_y_2, v200_z_2, col200_2] = ...
    textread('radius2.txt', '%f %f %f %f %f %f %f %f %f',10000);
[x200_disp_3, y200_disp_3, z200_disp_3, particle200_3, time200_3, v200_x_3,...
    v200_y_3, v200_z_3, col200_3] = ...
    textread('radius3.txt', '%f %f %f %f %f %f %f %f %f',10000);
[x_disp_s, y_disp_s, z_disp_s, particle_s, time_s, v_x_s, v_y_s, v_z_s, ...
 col_s] = textread('codeStraight.txt', '%f %f %f %f %f %f %f %f %f',10000);
%% Straigh flow alignment
for j = 1 : 34
   par = j - 1 ;
   loc_s = find(particle_s == par);
   for i = 1 : 17
        v_loc_xs (j,i) = v_x_s(loc_s(i));
        v_loc_ys (j,i) = v_y_s(loc_s(i));
        v_loc_zs (j,i) = v_z_s(loc_s(i));
        x_loc_xs (j,i) = x_disp_s(loc_s(i));
        x_loc_ys (j,i) = y_disp_s(loc_s(i));
        x_loc_zs (j,i) = z_disp_s(loc_s(i));
   end
end
%% Sinusoidal Alingment
for j = 1 : 50
    par = j-1;
    loc_1 = find(particle_1 == par);
    loc_2 = find(particle_2 == par);
    loc_3 = find(particle_3 == par);
    for i = 1 : 25
        v_loc_x_1 (j,i) = v_x_1(loc_1(i));
        v_loc_y_1 (j,i) = v_y_1(loc_1(i));
        v_loc_z_1 (j,i) = v_z_1(loc_1(i));
        x_loc_x_1 (j,i) = x_disp_1(loc_1(i));
        x_loc_y_1 (j,i) = y_disp_1(loc_1(i));
        x_loc_z_1 (j,i) = z_disp_1(loc_1(i));
        v_loc_x_2 (j,i) = v_x_2(loc_2(i));
```

```
        v_loc_y_2 (j,i) = v_y_2(loc_2(i));
        v_loc_z_2 (j,i) = v_z_2(loc_2(i));
        x_loc_x_2 (j,i) = x_disp_2(loc_2(i));
        x_loc_y_2 (j,i) = y_disp_2(loc_2(i));
        x_loc_z_2 (j,i) = z_disp_2(loc_2(i));
        v_loc_x_3 (j,i) = v_x_3(loc_3(i));
        v_loc_y_3 (j,i) = v_y_3(loc_3(i));
        v_loc_z_3 (j,i) = v_z_3(loc_3(i));
        x_loc_x_3 (j,i) = x_disp_3(loc_3(i));
        x_loc_y_3 (j,i) = y_disp_3(loc_3(i));
        x_loc_z_3 (j,i) = z_disp_3(loc_3(i));
    end
end
clear loc_1;
clear loc_2;
clear loc_3;
for j = 1 : 34
    par = j-1;
    loc_1 = find(particle200_1 == par);
    loc_2 = find(particle200_2 == par);
    loc_3 = find(particle200_3 == par);
    for i = 1 : 17
        v200_loc_x_1 (j,i) = v200_x_1(loc_1(i));
        v200_loc_y_1 (j,i) = v200_y_1(loc_1(i));
        v200_loc_z_1 (j,i) = v200_z_1(loc_1(i));
        x200_loc_x_1 (j,i) = x200_disp_1(loc_1(i));
        x200_loc_y_1 (j,i) = y200_disp_1(loc_1(i));
        x200_loc_z_1 (j,i) = z200_disp_1(loc_1(i));
        v200_loc_x_2 (j,i) = v200_x_2(loc_2(i));
        v200_loc_y_2 (j,i) = v200_y_2(loc_2(i));
        v200_loc_z_2 (j,i) = v200_z_2(loc_2(i));
        x200_loc_x_2 (j,i) = x200_disp_2(loc_2(i));
        x200_loc_y_2 (j,i) = y200_disp_2(loc_2(i));
        x200_loc_z_2 (j,i) = z200_disp_2(loc_2(i));
        v200_loc_x_3 (j,i) = v200_x_3(loc_3(i));
```

```
        v200_loc_y_3 (j,i) = v200_y_3(loc_3(i));
        v200_loc_z_3 (j,i) = v200_z_3(loc_3(i));
        x200_loc_x_3 (j,i) = x200_disp_3(loc_3(i));
        x200_loc_y_3 (j,i) = y200_disp_3(loc_3(i));
        x200_loc_z_3 (j,i) = z200_disp_3(loc_3(i));
    end
end
v_total_1  = sqrt(v_loc_x_1.^2 + v_loc_y_1.^2 + v_loc_z_1.^2);
v_total_2  = sqrt(v_loc_x_2.^2 + v_loc_y_2.^2 + v_loc_z_2.^2);
v_total_3  = sqrt(v_loc_x_3.^2 + v_loc_y_3.^2 + v_loc_z_3.^2);
v_total_s  = sqrt(v_loc_xs.^2 + v_loc_ys.^2 + v_loc_zs.^2);
v200_total_1  = sqrt(v200_loc_x_1.^2 + v200_loc_y_1.^2 + v200_loc_z_1.^2);
v200_total_2  = sqrt(v200_loc_x_2.^2 + v200_loc_y_2.^2 + v200_loc_z_2.^2);
v200_total_3  = sqrt(v200_loc_x_3.^2 + v200_loc_y_3.^2 + v200_loc_z_3.^2);
for i = 1 : 25
    l_diff_1 (i) = sqrt( (x_loc_x_1(1,i)-x_loc_x_1(1,1))^2 + ...
        (x_loc_y_1(1,i)-x_loc_y_1(1,1))^2 + ...
        (x_loc_z_1(1,i)-x_loc_z_1(1,1))^2 );
    l_diff_2 (i) = sqrt( (x_loc_x_1(2,i)-x_loc_x_1(2,1))^2 + ...
        (x_loc_y_1(2,i)-x_loc_y_1(2,1))^2 + ...
        (x_loc_z_1(2,i)-x_loc_z_1(2,1))^2 );
    l_diff_3 (i) = sqrt( (x_loc_x_2(1,i)-x_loc_x_2(1,1))^2 + ...
        (x_loc_y_2(1,i)-x_loc_y_2(1,1))^2 + ...
        (x_loc_z_2(1,i)-x_loc_z_2(1,1))^2 );
    l_diff_4 (i) = sqrt( (x_loc_x_2(2,i)-x_loc_x_2(2,1))^2 + ...
        (x_loc_y_2(2,i)-x_loc_y_2(2,1))^2 + ...
        (x_loc_z_2(2,i)-x_loc_z_2(2,1))^2 );
    l_diff_5 (i) = sqrt( (x_loc_x_3(1,i)-x_loc_x_3(1,1))^2 + ...
        (x_loc_y_3(1,i)-x_loc_y_3(1,1))^2 + ...
        (x_loc_z_3(1,i)-x_loc_z_3(1,1))^2 );
    l_diff_6 (i) = sqrt( (x_loc_x_3(2,i)-x_loc_x_3(2,1))^2 + ...
        (x_loc_y_3(2,i)-x_loc_y_3(2,1))^2 + ...
        (x_loc_z_3(2,i)-x_loc_z_3(2,1))^2 );
end
for i = 1 : 17
```

```
    l200_diff_1 (i) = sqrt( (x200_loc_x_1(1,i)-x200_loc_x_1(1,1))^2 + ...
        (x200_loc_y_1(1,i)-x200_loc_y_1(1,1))^2 + ...
        (x200_loc_z_1(1,i)-x200_loc_z_1(1,1))^2 );
    l200_diff_2 (i) = sqrt( (x200_loc_x_1(2,i)-x200_loc_x_1(2,1))^2 + ...
        (x200_loc_y_1(2,i)-x200_loc_y_1(2,1))^2 + ...
        (x200_loc_z_1(2,i)-x200_loc_z_1(2,1))^2 );
    l200_diff_3 (i) = sqrt( (x200_loc_x_2(1,i)-x200_loc_x_2(1,1))^2 + ...
        (x200_loc_y_2(1,i)-x200_loc_y_2(1,1))^2 + ...
        (x200_loc_z_2(1,i)-x200_loc_z_2(1,1))^2 );
    l200_diff_4 (i) = sqrt( (x200_loc_x_2(2,i)-x200_loc_x_2(2,1))^2 + ...
        (x200_loc_y_2(2,i)-x200_loc_y_2(2,1))^2 + ...
        (x200_loc_z_2(2,i)-x200_loc_z_2(2,1))^2 );
    l200_diff_5 (i) = sqrt( (x200_loc_x_3(1,i)-x200_loc_x_3(1,1))^2 + ...
        (x200_loc_y_3(1,i)-x200_loc_y_3(1,1))^2 + ...
        (x200_loc_z_3(1,i)-x200_loc_z_3(1,1))^2 );
    l200_diff_6 (i) = sqrt( (x200_loc_x_3(2,i)-x200_loc_x_3(2,1))^2 + ...
        (x200_loc_y_3(2,i)-x200_loc_y_3(2,1))^2 + ...
        (x200_loc_z_3(2,i)-x200_loc_z_3(2,1))^2 );
end
for i = 1 : 17
       l_diff_s1 (i) = sqrt( (x_loc_xs(1,i)-x_loc_xs(1,1))^2 + ...
        (x_loc_ys(1,i)-x_loc_ys(1,1))^2 + ...
        (x_loc_zs(1,i)-x_loc_zs(1,1))^2 );
       l_diff_s2 (i) = sqrt( (x_loc_xs(2,i)-x_loc_xs(2,1))^2 + ...
        (x_loc_ys(2,i)-x_loc_ys(2,1))^2 + ...
        (x_loc_zs(2,i)-x_loc_zs(2,1))^2 );
end
t = 0:5e-3:0.12;
t_s = 0:5e-3:0.08;
figure(1)
plot(t,l_diff_1,'-or')
hold
plot(t,l_diff_2,'-*r')
plot(t,l_diff_3,'-ob')
plot(t,l_diff_4,'-*b')
```

```
plot(t,l_diff_5,'-ok')
plot(t,l_diff_6,'-*k')
plot(t_s,l_diff_s1,'-oc')
plot(t_s,l_diff_s2,'-*c')
hold off
xlabel('Time (s)');
ylabel('Diffusion length of particle 100\mu m x 100\mu m (mm)');
legend('Case 1 - P1','Case 1 - P2','Case 2 - P1','Case 2 - P2',...
    'Case 3 - P1','Case 3 - P2','Straight P1','Straight - P2');
figure(2)
plot(t_s,l200_diff_1,'-or')
hold
plot(t_s,l200_diff_2,'-*r')
plot(t_s,l200_diff_3,'-ob')
plot(t_s,l200_diff_4,'-*b')
plot(t_s,l200_diff_5,'-ok')
plot(t_s,l200_diff_6,'-*k')
hold off
xlabel('Time (s)');
ylabel('Diffusion length of particle 120\mu m x 120\mu m (mm)');
legend('Case 4 - P1','Case 4 - P2','Case 5 - P1','Case 5 - P2', ...
    'Case 6 - P1','Case 6 - P2');
figure(3)
plot (t,x_loc_z_1(1,:),'-or')
hold
plot (t,x_loc_z_1(2,:),'-*r')
plot (t,x_loc_z_2(1,:),'-ob')
plot (t,x_loc_z_2(2,:),'-*b')
plot (t,x_loc_z_3(1,:),'-ok')
plot (t,x_loc_z_3(2,:),'-*k')
plot(t_s,x_loc_zs(1,:),'-oc')
plot(t_s,x_loc_zs(2,:),'-*c')
hold off
xlabel('Time (s)');
ylabel('Particle displacement in z-direction 100\mu m x 100\mu m (mm)');
```

```
legend('Case 1 - P1','Case 1 - P2','Case 2 - P1','Case 2 - P2',...
    'Case 3 - P1','Case 3 - P2','Straight P1','Straight - P2');
figure(4)
plot (t_s,x200_loc_z_1(1,:),'-or')
hold
plot (t_s,x200_loc_z_1(2,:),'-*r')
plot (t_s,x200_loc_z_2(1,:),'-ob')
plot (t_s,x200_loc_z_2(2,:),'-*b')
plot (t_s,x200_loc_z_3(1,:),'-ok')
plot (t_s,x200_loc_z_3(2,:),'-*k')
hold off
xlabel('Time (s)');
ylabel('Particle displacement in z-direction 120\mu m x 120\mu m (mm)');
legend('Case 4 - P1','Case 4 - P2','Case 5 - P1','Case 5 - P2', ...
    'Case 6 - P1','Case 6 - P2');
figure(5)
plot (t,v_total_1(1,:),'-or')
hold
plot (t,v_total_1(2,:),'-*r')
plot (t,v_total_2(1,:),'-ob')
plot (t,v_total_2(2,:),'-*b')
plot (t,v_total_3(1,:),'-ok')
plot (t,v_total_3(2,:),'-*k')
hold off
xlabel('Time (s)');
ylabel('Particle Velocity 100\mu m x 100\mu m (m/s)');
legend('Case 1 - P1','Case 1 - P2','Case 2 - P1','Case 2 - P2', ...
'Case 3 - P1','Case 3 - P2','Straight P1','Straight - P2');
figure(6)
plot (t_s,v200_total_1(1,:),'-or')
hold
plot (t_s,v200_total_1(2,:),'-*r')
plot (t_s,v200_total_2(1,:),'-ob')
plot (t_s,v200_total_2(2,:),'-*b')
plot (t_s,v200_total_3(1,:),'-ok')
```

```
plot (t_s,v200_total_3(2,:),'-*k')
hold off
xlabel('Time (s)');
ylabel('Particle Velocity 120\mu m x 120\mu m (m/s)');
legend('Case 4 - P1','Case 4 - P2','Case 5 - P1','Case 5 - P2', ...
    'Case 6 - P1','Case 6 - P2');
```

Appendix B

Recipe for Microchannel Production using Soft Lithography

1. Firstly manufactured mold should be cleaned with air gun to remove dust on the surface.
2. Then, PDMS was mixed with curing agent with 10:1 ratio (mass based) in a petri dish. Mixture should be scrambled with a tool until the mixture becomes completely homogeneous.
3. Petri dish was placed in vacuum chamber to remove air bubbles in the mixture. Average vacuum time takes 20 minutes.
4. Mixture was poured into the mold and putted into the vacuum chamber for an additional 10 minutes.
5. Mold was baked in the oven at 80°C. Material of the mold plays a critical role in this step. If the mold is based on Aluminum, baking time decreases to 45 minutes. If the mold is made of plexiglass or Si substrate, baking time reaches to 1 hour.
6. PDMS was peeled off from the mold. It is better to cut and remove edges first in order not to damage the device.

7. Holes were opened with the puncher.
8. To remove dust or particles on the surface, non-electrostatic tape was used.
9. Before exposing device under oxygen plasma, chamber was run until purple plasma light becomes visible.
10. PDMS device and lamel was placed inside the oxygen plasma chamber and exposed to UV for 30 seconds. Device should not be touching to the lamel during this process.
11. PDMS device was putted on the lamel and pushed from the top.
12. Test the device under microscope to check whether there is a congestion, insufficient bonding or leaking.

Appendix C

Mask of Cleanroom Fabrication

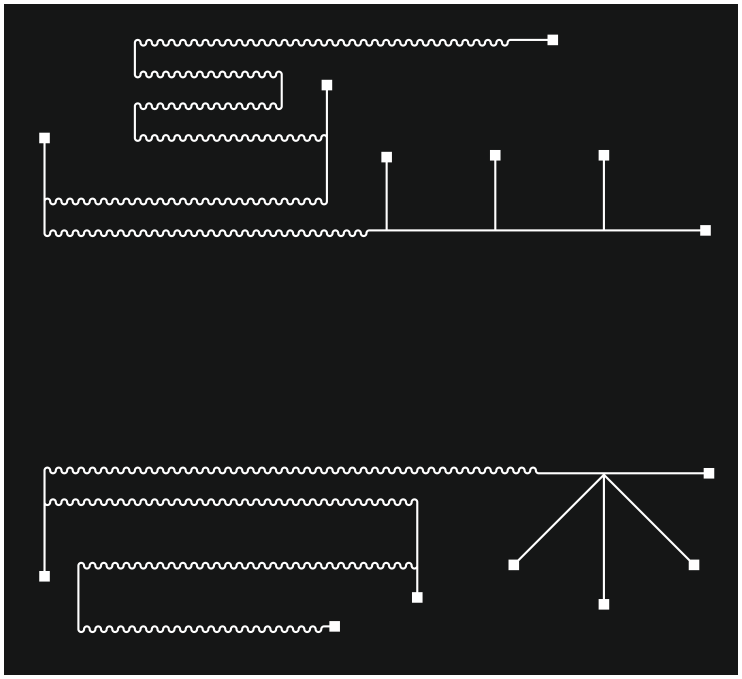

Figure C.1: Mask of microfluidic device